Regulation of the macrolide resistance ABC-F translation factor MsrD

Corentin R. Fostier[1], Farès Ousalem[1], Elodie C. Leroy[2], Saravuth Ngo[1], Heddy Soufari[2,3], C. Axel Innis[2], Yaser Hashem[2,*], Grégory Boël[1,4,*]

[1]Expression Génétique Microbienne, CNRS, Université Paris Cité, Institut de Biologie Physico-Chimique, 75005 Paris, France

[2]INSERM U1212 (ARNA), Institut Européen de Chimie et Biologie, Université de Bordeaux, 33607 Pessac, France

[3]Current address: NovAliX, Boulevard Sébastien Brant, Bioparc, 67405 Illkirch Cedex, France

[4]Lead contact

*Correspondence:

Grégory Boël, Institut de Biologie Physico-Chimique, 13 rue Pierre et Marie Curie, 75005 Paris, France, tel. : +33 (0) 1 58 41 51 21; e-mail: boel@ibpc.fr

Yaser Hashem, Institut Européen de Chimie et Biologie, Université de Bordeaux, 33607 Pessac, France, tel. : +33 (0) 5 40 00 88 22; e-mail: yaser.hashem@inserm.fr

SUMMARY

Antibiotic resistance ABC-Fs (ARE ABC-Fs) are translation factors currently proliferating among human pathogens that provide resistance against clinically important ribosome-targeting antibiotics. Here, we combine genetic and structural approaches to determine the regulation of *streptococcal* ARE ABC-F gene *msrD* in response to macrolide exposure and also demonstrate that MsrD twin-ATPase sites work asymmetrically to mediate the dynamic of MsrD interaction with the ribosome. We show that cladinose-containing macrolides lead to insertion of MsrDL leader peptide into an undocumented conserved crevice of the ribosomal exit tunnel concomitantly with 23S rRNA rearrangements that prevent peptide bond formation and preclude accommodation of release factors. The stalled ribosome obstructs formation of a Rho-independent terminator which prevents *msrD* transcriptional attenuation. This stalled ribosome is rescued by MsrD, but not by MsrD mutants which do not provide antibiotic resistance, showing evidence of equivalence between MsrD function in antibiotic resistance and its action on this complex.

KEYWORDS

Ribosome, protein synthesis, antibiotic resistance, ARE ABC-F protein family, leader peptide, cryo-EM.

INTRODUCTION

ABC-F ATPases belonging to the ATP-Binding Cassette (ABC) superfamily are translation factors and some of them, termed antibiotic resistance ABC-Fs (ARE ABC-Fs), confer resistance to clinically important antibiotics that bind to the ribosomal peptidyl transferase center (PTC) and/or the nascent peptide exit tunnel (NPET)[1–7]. ABC-F proteins are composed of two ABC domains (or Nucleotide Binding Domains, NBDs) joined by a linker region called P-site tRNA-interaction motif (PtIM)[8,9], also termed antibiotic resistance determinant (ARD) for ARE ABC-Fs[1–3]. The two ABC domains dimerize after binding of two ATP molecules and in this conformation the factor can bind the ribosomal E-site[9], where the PtIM adopts an α-helical hairpin conformation that interacts directly with the peptidyl-tRNA and extends toward the PTC/NPET. Three antibiotic resistance phenotypes are associated with ARE ABC-Fs: (i) MKS_B (Macrolides, Ketolides, Streptogramins group B); (ii) PLS_A (Pleuromutilins, Lincosamides, Streptogramins group A); (iii) PhO (Phenicols, Oxazolidinones)[10,11]. However, despite structural investigations[1–3,5,7], the exact molecular mechanism of action of ARE ABC-Fs remains unclear.

Over the last forty years, biochemical and structural investigations demonstrated the ability of elongating nascent chains (NC) into the ribosomal tunnel to interact with metabolites or antibiotics, thus adapting protein synthesis to environmental cues[12–16]. In human pathogens, antibiotic-dependent formation of stalled ribosome complexes (SRCs) on regulatory ORFs, named leader peptides, can subsequently allow regulation of downstream resistance genes in response to antibiotic exposure[17–20].

ARE ABC-F gene *msrD* is a member of the *msr* (macrolide and streptogramin B resistant) gene group previously referred as *mel*[21,22]. This gene is generally found in operon with a macrolide efflux facilitator (*mefA* or *mefE) gene*, the two corresponding proteins acting synergistically to confer macrolide resistance[23–26]. This operon is part of the Macrolide Efflux Genetic Assembly (MEGA)[27,28] that disseminates in human pathogens on mobile genetic elements: conjugative transposons like the tn916-type[29] and conjugative prophages like the Φ1207.3[30] among *Streptococci*, conjugative plasmids like the pMUR050 [31] among

67 *Enterobacteria*. In *Streptococci*, the operon is transcribed in presence of erythromycin (ERY)
68 as a polycistronic mRNA from a single promoter located ~350 bp upstream *mefA*[32,33]. It is also
69 regulated by ribosome-mediated transcription attenuation via MefAL leader peptide
70 (MTASMRLR), which is closely related to ErmDL leader peptide (MTHSMRLRFPTLNQ), both
71 polypeptides harboring the characteristic macrolide-arrest motif Arg/Lys-X-Arg/Lys so called
72 "+x+"[14,33–35].

73 Here, we report the presence of a second transcriptional attenuator on the *mefA/msrD*
74 operon regulating exclusively *msrD* expression upon macrolide exposure. Presence of ERY
75 induces ribosome stalling on the previously identified *msrDL* leader peptide (encoding
76 MYLIFM)[34], allowing RNA polymerase (RNAP) to bypass an intrinsic terminator. Our findings
77 demonstrate stalling occurs due to hampered translation termination on UAA stop codon,
78 action of both release factors 1 and 2 (RF1 and RF2) being inhibited. Our results are supported
79 by the cryo-EM structure of MsrDL-SRC that provides molecular insight on how the PTC
80 precludes productive accommodation of RF1/RF2 and how the NC discriminates tunnel-bound
81 cladinose-containing macrolides. The path of the NC within the tunnel greatly differs from
82 previously described leader peptides[12–16] with the NC latching into a ribosomal crevice,
83 conserved from prokaryotes to eukaryotes, delimited by 23S rRNA nucleotides U2584, U2586,
84 G2608 and C2610 that may form a novel ribosomal functional site. Finally, our results
85 demonstrate that the two ATPase sites of MsrD perform different functions and the protein can
86 negatively self-regulate its synthesis in presence of ERY by direct action on MsrDL-stalled
87 ribosomes.

88

89 **RESULTS**

90 **MsrD provides macrolide and ketolide resistance by direct interaction with ribosome**

91 The *mefA/msrD* macrolide resistance operon (Fig. 1a) is part of the MEGA element
92 currently spreading among clinical isolates and livestock[33,36–38]. A phylogenetical analysis
93 (Supplementary fig. 1a) shows that the operon disseminates predominantly in Gram-positive
94 firmicutes (mostly *Streptococci*) and in some Gram-negative proteobacteria (such as

95 *Haemophilus influenzae, Neisseria gonorrhoeae or Escherichia coli*). Gene *msrD* shares ~62
96 % identity with its closest homolog *msrE*[7], both factors exhibiting the canonical ABC-F
97 organization (Fig. 1b and Supplementary fig. 1b).

98 Model bacteria *Escherichia coli* (*E. coli)* presents undeniable advantages for genetic
99 and molecular biology, but presence of multidrug efflux systems greatly limits its use in
100 antibiotic research[39,40]. To circumvent this limitation, we took advantage of *E. coli* DB10 strain
101 which exhibits exacerbated sensitivity toward macrolide antibiotics[41]. Heterologous expression
102 of $msrD_{WT}$ from an arabinose-inducible promoter conferred macrolide and ketolide resistance
103 phenotype to *E. coli* DB10 strain (Table 1), demonstrating the functionality of the factor in this
104 organism. Expression of $msrD_{WT}$ resulted in 8-fold minimal inhibitory concentration (MIC)
105 increase for 14-membered macrolide ERY, 8-fold for 15-membered macrolide azithromycin
106 (AZI) and 2-fold for telithromycin (TEL, ketolide antibiotic derived from 14-membered
107 macrolides). Similar results were reported for *Streptococcus pneumoniae* clinical isolates[23].
108 However, no change in MIC was observed for 16-membered macrolides tylosin (TYL) and
109 spiramycin (SPI), neither for non-macrolide antibiotics lincomycin (LNC), linezolid (LNZ) and
110 retapamulin (RTP) (Table 1).

111 Comparison of polysome profiles from bacteria unexposed or exposed to ERY show a
112 stabilization of ribosome disomes (Fig. 1c, 1d and Supplementary fig. 1c) as expected for an
113 antibiotic that inhibits ribosome elongation. The disome accumulation likely results from
114 elongating ribosomes that collide on ERY-stalled ribosomes arrested at the beginning of the
115 coding sequence. In presence of ERY ribosomes preferentially stall when they encounter "+x+"
116 motifs which are present in the first 30 amino-acids of ~25% of *E. coli* proteins[42,43]. Expression
117 of $msrD_{WT}$ alleviates the accumulation of disomes and restores a profile identical to that without
118 ERY (Fig. 1d versus 1c and Supplementary fig. 1c). Western blots of the polysome fractions
119 show an $MsrD_{WT}$ association with the 70S ribosome and the 50S subunit and polysomes (Fig.
120 1d and Supplementary fig. 1c). These results agree with a model in which $MsrD_{WT}$ directly
121 rescues ERY-stalled ribosomes and that MsrD can restore normal translation in presence of
122 the antibiotic.

123 To understand the function of the ATPase activity of MsrD, we constructed ATPase-
124 deficient variants $MsrD_{E125Q}$, $MsrD_{E434Q}$ and $MsrD_{E125Q/E434Q}$ (hereafter referred as $MsrD_{EQ2}$) by
125 replacing the catalytic glutamic acid residue (E) in Walker B motif of each or both ABC domain
126 by a glutamine (Q) (Fig. 1b and Supplementary fig. 1b). This mutation strongly reduces the
127 ATP hydrolysis while preserving the local stereochemistry of active site and has been
128 extensively used to trap ABC-F factors on the ribosome in ATP-bound conformation[1–3,5,9].
129 Expression of *msrD*$_{EQ2}$ in absence of ERY inhibits cell growth after OD_{600}=0.4 and shows an
130 accumulation of disomes on polysome profile (Supplementary fig. 1c) and western-blotting
131 reveals its association with the 30S subunit, 70S ribosome and polyribosomes (Fig. 1d and
132 Supplementary fig. 1c). These results shows that $MsrD_{EQ2}$ binds to the ribosome and inhibits
133 its elongation as observed for most of the ABC-F carrying the E-to-Q mutation[8,44]. In presence
134 of ERY, the disome and trisome accumulation increases and western blots show an increase
135 of $MsrD_{EQ2}$ in the disome fraction (Fig. 1d and Supplementary fig. 1c). Still, the ATPase activity
136 of MsrD impacts its binding preferences, $MsrD_{WT}$ interacting more with the 50S subunit in
137 contrast to $MsrD_{EQ2}$ interacting more with the 70S ribosome (Fig. 1d and Supplementary fig.
138 1c). Interestingly, the $MsrD_{E125Q}$ variant has an interaction profile with the ribosome similar to
139 $MsrD_{WT}$ whether $MsrD_{E434Q}$ has one closer to $MsrD_{EQ2}$.

140 A model consistent with these observations would imply that $MsrD_{WT}$ binds to ERY-
141 stalled ribosomes in an ATP-bound close conformation without the need of its ATPase activity,
142 then ATPase activity triggers 70S dissociation, $MsrD_{WT}$ staying associated with the 50S
143 subunit. Similar results were observed by expressing *msrD*$_{WT}$ and *msrD*$_{EQ2}$ in *E. coli* K12
144 MG1655 (Supplementary fig. 1d) in absence of ERY and with chloramphenicol being added to
145 stabilize polysomes. They also show a decrease of the 70S peak correlated with an increase
146 of 30S and 50S peaks for *msrD*$_{WT}$ condition when compared to the control, supporting the
147 proposed dissociation model. Western blots show more $MsrD_{EQ2}$ than $MsrD_{WT}$ in soluble
148 lysates (Supplementary fig. 1c) but $MsrD_{EQ2}$ inhibits protein synthesis including its own
149 synthesis. Therefore, we hypothesized that $MsrD_{EQ2}$ is less expressed but more soluble, which
150 has been confirmed with a solubility test (Supplementary fig. 1e).

151 We evaluated the influence of E-to-Q mutations of MsrD on bacterial growth and
152 antibiotic resistance phenotype. All the mutations impair bacterial growth and antibiotic
153 resistance phenotype (Fig. 1e), while $MsrD_{E125Q}$ and $MsrD_{EQ2}$ have a similar effect on bacterial
154 growth in absence or at low ERY concentration, $MsrD_{E434Q}$ is more toxic. However, $MsrD_{E125Q}$
155 variant maintains some resistance (MIC = 4 μM) compared to control (MIC = 2 μM) which is
156 also supported by the fact that $MsrD_{E125Q}$ IC_{50} is ~8 times higher than Control IC_{50} (Fig. 1e and
157 Supplementary Table 1). These results together with polysome profile experiments (Fig. 1c,
158 1d and Supplementary fig. 1d) suggest that interaction of MsrD with the 50S is necessary for
159 antibiotic resistance mechanism.

160 The two ATP hydrolysis sites (Supplementary fig. 1b) have therefore different tasks
161 and are functionally asymmetric, ATP site II achieving in part the mechanism of ERY-stalled
162 ribosome rescue. We also evaluated the importance of other residues of MsrD. Truncation of
163 the PtIM (replaced by three glycine) or just the Loop (ΔPtIM, ΔLoop respectively) completely
164 abolished the resistance phenotype *in vivo* (Fig. 1f) as reported *in vitro* for MsrE[7]. Punctual
165 mutations in the Loop (Fig. 1b) affect the resistance phenotype to a different extent, mutation
166 of R241 into alanine has almost no effect on the phenotype, but equivalent mutation for L242
167 or H244 reduces IC_{50} by ~3 fold (Fig. 1g and Supplementary Table 1), demonstrating that these
168 residues are important for MsrD function, but not essential even if they are predicted at the
169 vicinity of the antibiotic (Supplementary fig. 1f) in the MsrE-ribosome complex[7]. Interestingly,
170 this finding contrasts with mutagenesis assays for MsrE showing that mutation R241A reduces
171 the resistance by more than 50%. Replacement of H244 by the larger residue tryptophan
172 should displace the drug by steric occlusion, but the variant lost most of its antibiotic resistance
173 phenotype (Fig. 1g). Similarly, $MsrD_{WT}$ does not provide resistance to TYL nor SPI (Table 1),
174 while both antibiotics should clash with MsrD according to MsrE structure (Supplementary fig.
175 1f). Same observation can be made with LNC, LNZ or RTP (Table 1 and Supplementary fig.
176 1f). Therefore, MsrD action on the antibiotic is indirect and direct steric occlusion to displace
177 the antibiotic seems excluded.

178

179 **Ribosome-mediated transcriptional attenuation regulates *msrD* expression**

180 Analysis of the *mefA/msrD* operon sequence exposes a stringent ribosome binding site
181 (RBS, whose sequence is 5'-GGAGGA-3') only 8 bp downstream *mefA* stop codon and
182 possibly required for translation of the downstream putative small ORF *msrDL* (Supplementary
183 fig. 2a). In order to test the influence of *msrDL* on *msrD* expression, a fluorescent reporter,
184 which contains the sequence spanning from the first nucleotide downstream *mefA* stop codon
185 to *msrD* three first codons fused to the Yellow Fluorescent Protein gene (YFP), was cloned in
186 the low copy pMMB plasmid[45] under the control of IPTG-inducible $P_{LlacO-1}$ promoter[46]. The
187 resulting plasmid, pMMB-*msrDL-msrD*$_{(1-3)}$:*yfp,* was used to directly follow the fluorescence
188 reflecting *yfp* expression (Fig. 2a).

189 Basal fluorescence level was found stable in *E. coli* DB10 strain containing pMMB-
190 *Control* independently of ERY concentration (Fig. 2a) while a fluorescence increase correlated
191 with ERY concentration was observed in cells containing pMMB-*msrDL-msrD*$_{(1-3)}$:*yfp*,
192 indicating an ERY-dependent induction. Optimal induction was found at 100 nM ERY while
193 only 6.25 nM was sufficient to significantly induce *msrD*$_{(1-3)}$:*yfp* expression, demonstrating the
194 high sensitivity of the system toward its inducer. A reduced, but significative fluorescence
195 signal was detected at 0 nM ERY indicating an imperfect repression of the regulation .
196 Inactivation of *msrDL* ORF by replacement of the start codon by an amber stop codon (pMMB-
197 *msrDL*$_{(no_ORF)}$-*msrD*$_{(1-3)}$:*yfp*) resulted in the elimination of the fluorescence induction (Fig. 2a),
198 demonstrating that *msrDL* translation is an important and necessary cis-acting feature to
199 regulate *msrD*$_{(1-3)}$:*yfp* expression as reported for *ermC*[47].

200 In bacteria, antibiotic-dependent gene induction relies mainly on translational or
201 transcriptional attenuation[48]. To determine if *msrDL* prompts a transcriptional or translational
202 attenuation, northern blots analysis with a probe located in *msrD*$_{(1-3)}$:*yfp* 3' UTR were performed
203 on total RNA extracted from cell exposed or not to ERY and/or IPTG. A 1.2-kb band
204 corresponding to *msrDL-msrD*$_{(1-3)}$:*yfp* mRNA is transcribed in presence of IPTG and starts to
205 increase steadily 5 min after exposure to 100 nM ERY (Fig. 2b). Consistent with this ERY-

206 dependent transcript accumulation, we concluded that *msrD* regulation by *msrDL* occurs at
207 the transcription level.

208 Transcription attenuation employs premature transcription termination via: (i) Rho-
209 dependent terminator (RDT) by binding of Rho factor, a RecA-type ATPase, to a C-rich and
210 G-poor sequence known as Rho utilization site[49]; (ii) Rho-independent terminator (RIT) where
211 a stable GC-rich stem-loop followed by a poly-uridine sequence causes RNAP to drop off[50].
212 Treatment with bicyclomycin, a Rho inhibitor, did not result in constitutive expression of the
213 reporter, thus excluding the possibility of RDT attenuation (Supplementary fig. 2b). Analysis of
214 the intergenic region between *msrDL* and *msrD* using ARNold server[51] revealed the presence
215 of a RIT with a ΔG of -7.9 kcal.mol^{-1}. We also identified a consensus TTNTTT NusG-dependent
216 RNAP pausing site embedded in *msrDL* sequence (Fig. 2c and Supplementary fig. 2a), as
217 previously described for *vmlR* [52,53]. In order to test this possible transcription termination
218 activity, we generated a mutant by removing the putative terminator (referred as pMMB-
219 msrDL$_{(no_term)}$-msrD$_{(1-3)}$:*yfp*). Deletion of the terminator resulted in a constitutive expression of
220 the fluorescent reporter in absence of ERY, indicating that the terminator is a necessary cis-
221 acting regulatory feature that can terminate transcription (Fig. 2c). These results validate the
222 presence of a second transcriptional attenuator in the *mefA*/*msrD* operon that regulates
223 exclusively *msrD*.

224

225 **Selective drug-sensing by MsrDL prevents its translation elongation and termination**

226 To determine how this regulation occurs via ribosome-mediated mechanism,
227 translation of *msrDL* mRNA with the PURE system[54] was subjected to various antibiotics and
228 its propensity to form SRC was analyzed by toeprinting[55] (Fig. 3 and Supplementary fig. 3). A
229 strong toeprint signal was observed in presence of ERY and AZI, while it was absent in
230 presence of TEL, TYL and SPI (Fig. 3a). This *in vitro* result is correlated to *in vivo* observations
231 made with the *msrD*$_{(1-3)}$:*yfp* reporter gene which was also only induced by ERY and AZI, but
232 not by TEL, TYL, SPI and non-macrolide antibiotics (Fig. 3b).

233 We further characterized the translation of *msrDL* mRNA and showed that in presence
234 of 50 µM RTP, an inhibitor of the first peptide bond formation which allows to identify ORFs
235 start codon[56], a clear toeprint occurred (Fig. 3c). This toeprint corresponds to a ribosome
236 stalled with the initiating codon in the ribosomal P site and confirms that ribosomes can initiate
237 *msrDL* translation. The toeprint observed at positions +31, +32 and +33 relative to *msrDL* 5'
238 end (Fig. 3a and 3c) in presence of ERY and AZI indicates an SRC located at the termination
239 step of MsrDL synthesis with the C-terminal methionine (M6) codon in the P site and UAA stop
240 codon in the A site. In accordance with this, reactions depleted of release factors (RF1, RF2,
241 RF3) (Fig. 3c) show the same toeprint result. Moreover, addition of puromycin led to the loss
242 of this toeprint signal, while preserving it in presence of ERY (Fig. 3c). Puromycin is an
243 aminonucleoside antibiotic mimicking A site substrate tyrosyl-tRNA and causing premature
244 chain termination. While actively translating ribosomes are sensitive to this antibiotic, stalled
245 ones tend to be refractory[15,16,20,57,58]. The resistance of MsrDL-SRC to puromycin is consistent
246 with an ERY-sensing NC that leads to PTC silencing and stalling. The stalled ribosome on
247 ORF *msrDL* covers the first half of the hairpin of the RIT and therefore prevents its formation
248 and transcription termination (Fig. 2c and Supplementary fig. 3).

249 The main dissimilarity between tested macrolides resides in the presence or absence
250 of a cladinose moiety on C3 of the macrocyclic lactone ring which appears to be critical for
251 MsrDL-SRC formation (Fig. 3a) similarly to ErmCL[20,59]. Absence of significant toeprint in
252 presence of TEL (whose C3 cladinose sugar is replaced by a keto group) suggests that *msrDL*
253 is translated efficiently without stalling. TYL and SPI differ from the other macrolides by the
254 presence of disaccharide mycaminose-mycarose in place of the C5 monosaccharide
255 desosamine. When bound to the ribosome, this extended sugar moiety protrudes into the PTC
256 of the ribosome[60]. Absence of intermediate toeprint and increase of the toeprint corresponding
257 to initiation complex in presence of these two drugs imply that these antibiotics stabilize the
258 initiation complex. Previous results[60–62] have shown that they inhibit the formation of the
259 peptide bond, our result suggests that it occurs mainly for the first peptide bond formation (Fig.
260 3a).

261 We submitted the sequence of MsrDL to an alanine-scanning to investigate the
262 importance of each residue and their ability to induce *msrD*$_{(1-3)}$:*yfp* reporter, which indirectly
263 reports the formation of an ERY-dependent SRC. The scan shows a strong reduction of
264 inducibility for all the mutated residues with the exception Y2 (Fig. 3d). Since MsrDL is a
265 hexapeptide, it is evident that most of the amino acids would have their importance to maintain
266 a conformation able to sense ERY. A complete loss of inducibility has been observed for
267 residues L3 and I4 suggesting that these two residues were directly involved in drug-sensing,
268 which was structurally confirmed and detailed in the next section. Moreover, considering that
269 MsrDL inhibits the action of both RF1/RF2 in presence of ERY, we mutated UAA stop codon
270 into RF1-specific UAG and RF2-specific UGA stop codons to investigate a putative preferential
271 inhibition as previously shown for TnaC[63]. Mutation of UAA into UAG or UGA reduces the level
272 of inducibility of the reporter gene (Supplementary fig. 2c) demonstrating the importance of the
273 stop codon. This observation is corroborated by our phylogenetic analysis which revealed a
274 large prevalence of UAA stop codon among the different *msrDL* variants (Supplementary fig.
275 2a). Most likely the UAA stop codon has been selected by evolution to maximize *msrD*
276 expression in presence of an inducer. Mutagenesis of *msrDL* sequence by synonymous
277 codons (iso-codons) as described in Methods leads to a reduction of the *yfp* expression for
278 MsrDL$_{WT-iso}$ construct, possibly due to the lack of NusG pausing site, but the regulation is mostly
279 preserved (Fig. 3d). Therefore, the amino acid composition of the peptide is responsible for
280 the ribosome stalling. Addition of an extra alanine before the stop codon in MsrDL$_{7A-iso}$
281 construct reduces the regulatory potential of the leader peptide (Fig. 3d). Toeprinting assay
282 reveals that this construct has two stalling positions: one occurs with the additional A7 codon
283 in the ribosomal A site and the second with the stop codon in the A site (Fig. 3e). Thus, MsrDL
284 peptide seems to induce efficient ribosomal stalling by preventing elongation and termination.
285 When both are uncoupled like in the MsrDL$_{7A-iso}$ construct the regulation is less efficient (Fig.
286 3d).

287 **Molecular mechanism of ribosome stalling by MsrDL**

288 To understand how MsrDL inhibits translation termination in presence of ERY, a
289 synthetic mRNA containing a single *msrDL* copy was translated *in vitro* with purified *E. coli*
290 DB10 ribosomes in presence of ERY as described in Supplementary fig. 4a and the resulting
291 sample was subjected to cryo-EM. Single-particle reconstruction of MsrDL-SRC was done by
292 refining two subclasses, one containing only P-tRNAS and one containing P- and E-tRNAs
293 (respectively 11% and 28.1% of total particles), as described in Methods and on
294 Supplementary fig. 4b. It resulted an initial map of 70S ribosome (EMD-13805) with an average
295 resolution of 3.0 Å that was subjected to multibody refinement, generating reconstructions for
296 the body and the head of the small subunit (EMD-13807 and EMD-13808) and the large
297 subunit (EMD-13806), presenting average resolutions of 3.08, 3.3 and 2.97 Å respectively
298 (Supplementary fig. 4b and 4c and Supplementary Table 2). The resolutions of the derived
299 reconstructions were consistent with clear and unambiguous assignment of ribosomal proteins
300 side chains, rRNA nucleotides and some post-transcriptional modifications (Supplementary
301 fig. 4d to 4f). Local resolution of the codon-anticodon allowed unambiguous identification of
302 the P-tRNA as an elongator $_{Met}$tRNA^{Met} (Supplementary fig. 4e), which is also confirmed by the
303 presence of distinctive elements such as N^4-acetylcytidine at position 34 (ac^{4}C34) and N^6-
304 threonylcarbamoyladenosine at position 37 (t^{6}A37) (Supplementary fig. 4e and 4f)[64,65],
305 consistently with the toeprint results which assigned the M6 codon in the P site and UAA stop
306 codon in the A site (Fig. 3c).

307 A clear density corresponding to ERY bound in its canonical position was found at the
308 entrance of the NPET (Fig. 4a, 4b and Supplementary fig. 4d), allowing clear attribution of
309 macrocyclic lactone ring, cladinose and desosamine sugars. A continuous density at the 3'
310 end of P-tRNA extending within the entrance of ribosome tunnel was identified as MsrDL-NC
311 and local resolution of ~3 Å allowed to model the peptide *de novo* (Fig. 4b and Supplementary
312 fig. 4d). It adopts a hook-like shape with its N-terminal extremity protruding into a cavity at the
313 entrance of the tunnel delimited by 23S rRNA nucleotides U2584, U2586, G2608 and C2610
314 (Fig. 4b). One noticeable feature of MsrDL interaction with the ribosome is its residue Y2 that

315 bulges out the base U2584 to form a π-stacking with the base G2583 (Fig. 4c and 4d) in place
316 of U2584. This unique interaction should stabilize the peptide conformation, while it appears
317 structurally significant, it is not strictly essential since replacement of the Y2 by an alanine
318 reduces by less than 50% the induction of the reporter gene (Fig. 3d). In addition, this residue
319 is substituted in some MsrDL variants (Supplementary fig. 2a). MsrDL does not show
320 numerous significant electrostatic interactions with the ribosome since it is mostly composed
321 of hydrophobic amino acids. It is likely stabilized by hydrophobic interactions.

322 Our biochemical investigations showed that MsrDL-SRC was formed due to hampered
323 translation termination on UAA stop codon. This stop codon is recognized by both RF1 and
324 RF2 which subsequently catalyze peptide hydrolysis via their conserved GGQ motif protruding
325 within the PTC. Structural alignment of our model to RF1- and RF2-containing ribosome
326 structures[66] revealed that proper accommodation of the RFs is prevented by steric clashes of
327 the methylated glutamine and the following glycines of the GGQ motif with the residue F5 of
328 MsrDL and 23S rRNA bases U2584 and U2585 respectively (Fig. 4e). The conformation of
329 MsrDL peptide stabilizes the PTC in an uninduced conformation[67] which prevents the opening
330 of the active site necessary for peptide bond formation and hydrolysis (Fig. 4f). This
331 observation suggests that MsrDL-SRC cannot catalyze peptide bond formation, as confirmed
332 by the toeprinting preformed on the $MsrDL_{7A\text{-}iso}$ construct (Fig. 3e). Structural alignment of
333 MsrDL-SRC with ErmBL- and ErmCL-SRC demonstrates that 23S rRNA nucleotides U2506
334 and 2585 are not in the same conformation (Supplementary fig. 5a and 5b), these bases in
335 MsrDL-SRC being in a conformation more similar to ErmDL-, SpeFL- and TnaC(R23F)-SRC
336 (Supplementary fig. 5c to 5e)[12–16]. However, unusual position of base U2584 seems to be a
337 unique feature of MsrDL-SRC.

338 MsrDL may monitor the presence of cladinose-containing drugs as our *in vivo* and *in*
339 *vitro* experiments suggested. Mutation of residues L3 and I4 abolished induction of the reporter
340 gene suggesting that they were critical for drug recognition and/or conformation of the peptide
341 (Fig. 3d). Consistently, in our model we identified residue L3 as the closest amino acid from
342 cladinose moiety and residue I4 as the closest from desosamine moiety (Fig. 4b and 4g).

343 However, similarly to ErmBL, no close contact between the nascent chain and the drug was
344 observed[13,68], residue L3 being ~3.8 Å away from cladinose sugar and residue I4 being ~3.9
345 Å away from desosamine sugar, consistently with a hydrophobic interaction between MsrDL
346 and the drug (Fig. 4g to 4i). This observation is also corroborated by previous descriptions of
347 pentapeptides conferring ERY resistance in which the presence of a leucine or isoleucine at
348 position 3 was critical for drug recognition[69,70]. Moreover, the importance of 23S rRNA residue
349 A2062 in acting as an ERY-sensor and in contributing to silence the PTC, has been
350 demonstrated for some regulatory leader peptides[71,72]. In the case of ErmCL, the critical
351 feature for macrolide-dependent stalling is the rotation of the base A2062 that forms an
352 Hoogsteen base pairing with m^2A2503[12,71,72]. The structure of MsrDL-SRC shows that residue
353 I4 restrains rotation of base A2062 (Fig. 4j). Therefore, MsrDL induces an A2062/m^2A2503-
354 independent ribosome stalling[72].

355 The path of MsrDL-NC within the ribosomal tunnel contrasts from all previous
356 descriptions of elongating polypeptides (Fig. 4b and 5). Indeed, ERY-sensing ErmBL, ErmCL
357 and ErmDL leader peptides[12–14] engage in the NPET and skirt around ERY, while MsrDL
358 curves before encountering the ligand then engages into a dead-end crevice at the entrance
359 of NPET (Fig. 4b and 5b). The same observation (Fig. 5c) can be made with metabolite-
360 sensing SpeFL/TnaC(R23F) leader peptides[15,16] which avoid the crevice and enter the NPET.
361 The first methionine of MsrDL-NC latches into the dead-end crevice which is delimited by 23S
362 rRNA nucleotides U2584, U2586, G2608 and C2610 (Fig. 5a to 5c). This crevice located at
363 the base of helix 93 (h93) is part of domain V of 23S rRNA and is conserved from bacteria to
364 human (mitoribosome and cytosolic ribosome) (Fig. 5d, Supplementary fig. 5f and 5g). We
365 named it proximal crevice.

366

367 **MsrD negatively regulates its own expression**

368 MsrD protein provides antibiotic resistance by rescuing ERY-stalled ribosome while
369 *msrDL* translation in presence of ERY leads to the formation of a SRC. If MsrD is also able to
370 rescue this SRC, it will repress its own expression and form a feedback loop similarly to Vga(A)

371 [73]. We tested this hypothesis using *E. coli* DB10 strains double transformed with pMMB-*msrDL-*
372 *msrD*$_{(1-3)}$:*yfp* and the compatible pBAD plasmid expressing various *msrD* variants. Strains were
373 grown in presence of ERY at 300 nM with their optical density and fluorescence monitored
374 (Fig. 6a). Strain carrying the pBAD-*Control* showed high fluorescence and low OD_{600} as
375 observed in Fig. 2a**,** reflecting an induction of the reporter and a susceptibility to ERY. On the
376 contrary, expression of *msrD* led to higher cell growth and a strong reduction of fluorescence
377 which correspond respectively to antibiotic resistance and repression of the expression of the
378 reporter. These results support that MsrD can rescue MsrDL-SRC and therefore releases the
379 RIT repressing *msrD* transcription.

380 The strain expressing *msrD*$_{E125Q}$ has a low ERY resistance (Fig. 1e). When it is co-
381 transformed with the pMMB-*msrDL-msrD*$_{(1-3)}$:*yfp* plasmid, no resistance is observed, possibly
382 because the presence of the two plasmid creates some toxicity. Overall, the results show that
383 MsrD variants that lost the ability to provide antibiotic resistance (ΔPtIM, ΔLoop and ATPase
384 deficient mutants) also lost the ability to rescue MsrDL-SRC (Fig. 6a). Point mutations in the
385 Loop of the PtIM indicated some discrepancy between antibiotic resistance phenotype and
386 MsrDL-SRC rescue. All the mutants show an intermediary phenotype with less antibiotic
387 resistance and less repression of reporter compared to MsrD. The mutant $MsrD_{H244w}$ has the
388 same repression effect on the reporter than $MsrD_{H244A}$ for an equivalent OD_{600} but it provides
389 more that 3 times less antibiotic resistance (Fig. 1g and 6a). The mutant $MsrD_{R241A}$ which
390 provides a resistance close to MsrD does not rescue the MsrDL-SRC as efficiently as the latter
391 one (Fig. 1g and 6a). Mutants $MsrD_{L242A}$ and $MsrD_{H244A}$ provide similar resistance, but
392 $MsrD_{H244A}$ confers a stronger repression of the reporter (Fig. 1g and 6a). Together these
393 observations demonstrate that the determinants of the dual function of MsrD in conferring
394 antibiotic resistance and rescuing MsrDL-SRC are overall similar.

395

396 **DISCUSSION**

397 We used genetic, molecular biology and structural approaches to dissect the regulation
398 of streptococcal ARE ABC-F gene *msrD*, its effect on ERY-stalled ribosomes and to provide

399 information on ARE ABC-F mechanisms of action. We characterized the *msrDL* regulatory
400 ORF which induces ribosome stalling in presence of cladinose-containing macrolides (Fig. 3,
401 4 and 6b). Our structural data show that this inhibition results from the conjoint effects of: (*i*)
402 MsrDL maintaining 23S rRNA bases U2506 and U2585 in an uninduced conformation (Fig.
403 4f), (*ii*) the steric occlusion by U2584, U2585 and MsrDL residue F5 that precludes the
404 productive accommodation of RF1/RF2 (Fig. 3c and 4e). MsrDL-stalled ribosome then
405 hampers formation of a RIT allowing transcription of *msrD* (Fig. 2c, 3a, 3c and 6b). The
406 coupling between translation and transcription necessary for this mechanism in *Streptococci*
407 is possibly mediated by a NusG-dependent RNAP pausing site in *msrDL* (Fig. 2c).

408 MsrD binds with some specificity to ERY-stalled ribosome (Fig. 1d) and then its ATPase
409 activity drives mechanical rearrangements to rescue stalled ribosome. The ATPase
410 mechanism that allows the rescue is still unknown for ARE ABC-Fs and all the current
411 structures of an ARE ABC-F in complex with the ribosome were generated with an ATPase-
412 dead mutant[1–3,5] or use of non-hydrolysable ATP analogues[7]. These structures do not capture
413 an antibiotic stalled complex and embodies a reaction intermediate before or after antibiotic
414 release of an ARE ABC-F trapped on the ribosome. We provide here some evidence about
415 possible mechanisms (Fig. 6b). We show that only one active ATPase site (Site II, $MsrD_{E125Q}$)
416 can provide some antibiotic resistance (Fig. 1e) while generating a strong toxicity for the cell
417 independently of the antibiotic and also shows more association with 50S (Fig 1c and 1d). The
418 mutant of Site II ($MsrD_{E434Q}$) shows a stronger toxicity (Fig. 1e) and no antibiotic resistance,
419 effects related to less dissociation from the ribosome (Fig. 1c and 1d). Therefore, it is possible
420 that site I is needed for complete dissociation of MsrD from the ribosome or subunits after ATP
421 hydrolysis occurs at site II. Mutation of both sites ($MsrD_{EQ2}$) leads to the same toxicity as for
422 inactive Site I (Fig. 1e), suggesting that having only Site II mutated induces a new MsrD
423 conformation that inhibits more cell growth. In accordance with these results, independent E-
424 to-Q mutations in the ARE ABC-F Vga(A), show that mutation in site I maintains an higher
425 ATPase activity than mutation in site II[74].

426 We envision two putative non-exclusive scenarios that involve for the first one, a
427 disassembling of ERY-stalled ribosomes, and for the other one, a displacement of the drug
428 followed by a restart of the translation process (Fig. 6b). A key point for future studies will be
429 to explore the ATPase activity of MsrD in a stalled-ribosome context to determine how many
430 rounds of ATP hydrolysis are necessary to rescue the latter one. The dissociation model
431 requires the hydrolysis of only two ATP molecules, while antibiotic displacement may require
432 multiple hydrolysis rounds in Site II to displace the drug and to position back the elongating
433 peptide in a correct conformation in the NPET. So far, those experiments have been
434 challenging due to the low solubility of all the ARE ABC-F proteins[2,6].

435 Alongside with ErmBL, ErmCL and ErmDL, MsrDL constitutes the fourth ERY-sensing
436 NC structurally described, however some mechanisms of drug-sensing and PTC silencing
437 differ. First, similarly to ErmCL, the presence of C3 cladinose sugar is required for stalling (Fig.
438 3a and 3b) contrary to ErmBL and ErmDL that senses drugs lacking this moiety such as
439 oleandomycin, solithromycin or telithromycin[12,14,59,68]. Second, similarly to ErmBL, no close
440 contact between the drug and MsrDL was observed (Fig. 4h and 4i)[68]. Third, MsrDL is the only
441 described leader peptide that exploits inhibition of its hydrolysis by RFs to induce stalling in
442 presence of antibiotic, similarly to the metabolite sensors TnaC and SpeFL[15,16]. On the
443 contrary, ErmBL[13], ErmCL[12] and ErmDL[14] employ only elongation inhibition. Fourth, ERY-
444 dependent stalling on *msrDL* regulates downstream *msrD* via transcriptional attenuation (Fig.
445 2b and 2c) while it relies on translational attenuation for ErmBL, ErmCL and ErmDL[14,68,75].
446 Finally, MsrDL-NC conformation and path within the ribosome greatly differ from previously
447 described ligand-sensing leader peptides that elongate within the tunnel (Fig. 5b and 5c)[12–16].
448 It adopts a hook-like shape possibly due to hydrophobic interactions with the drug (Fig. 4b, 4g
449 and 4h), while its initiating methionine engages in a dead-end crevice at the NPET entrance
450 (Fig. 5). To our knowledge, this is the first description of this crevice, conserved in prokaryotes
451 and eukaryotes (Supplementary fig. 5f and 5g), as a functional site within the ribosome and
452 we propose to name it proximal crevice.

453 ARE ABC-F genes tend to be transcriptionally regulated as illustrated by *msrD*, *vmlR*,
454 *vgaA*, *lmo0919* and *lmrC*[52,73,76–78]. However, MsrD can regulated its own expression by creating
455 a negative feedback-loop which is not the case for VmlR[52]. The gene *msrD* forms an operon
456 with the efflux pump *mefA* (Fig. 1a) which is also regulated *via* ribosome-mediated
457 transcriptional attenuation, translational stalling occurring on *mefAL*[33]. Therefore, *msrD* is
458 under the dual-regulation of two ERY-sensing leader peptides. One explanation for this
459 redundancy may reside in the need for the bacteria to tightly regulate *msrD* because of its
460 toxicity. Expression of $msrD_{WT}$ in *E. coli* DB10 led to a 20 % growth defect compared to control
461 condition (Fig. 1e) suggesting that $msrD_{WT}$ expression has a fitness cost for the bacteria and
462 can be beneficial only in presence of antibiotic. The presence of two attenuators creates a
463 double-lock system to avoid any basal expression in absence of inducer and the negative
464 feedback-loop maintains a minimal amount of MsrD production. Thus, as long as MefA can
465 export enough antibiotic to provide resistance, *msrD* should be kept repressed. The fitness
466 cost of the expression of ARE ABC-F genes is possibly the Achilles heel of bacteria containing
467 those genes and may be exploited to fight antibiotic resistance. MsrD provides resistance to
468 ERY, AZY and TEL[23] (Table 1) but only the first two induce its expression, indicating that MsrD
469 can provide some resistance for an antibiotic which does not induce its expression. Thus,
470 MsrDL facilitates the use of MsrD by the bacteria and maintains its evolution under its control.
471

ACKNOWLEDGMENTS

This work has benefited from the facilities and expertise of the Biophysical and Structural Chemistry platform (BPCS) at IECB, CNRS UMS3033, Inserm US001, University of Bordeaux. C.R.F. is funded by a doctoral grant from the french Ministère de l'Enseignement supérieur, de la Recherche et de l'Innovation, F.O. and G.B. have received support from the LABEX program (DYNAMO ANR-11-LABX-0011), and the ANR grants EZOtrad (ANR-14-ACHN-0027) for G.B. and ABC-F_AB (ANR-18-CE35-0010) for G.B. and Y.H., ERC-2017-STG #759120 "TransTryp" to Y.H. E.C.L. and C.A.I. have received funding for this project from the European Research Council (ERC) under the European Union's Horizon 2020 research and innovation program (Grant Agreement No. 724040). Authors would like to thank Dr. Olivier Chesneau (Département de Microbiologie, Institut Pasteur, Paris - France) for providing *E. coli* DB10 strain, plasmids pBAD33 and pVN50; Dr. Sylvain Durand and Dr. Maud Guillier (UMR 8261, CNRS, Université de Paris, Institut de Biologie Physico-Chimique, Paris - France) that kindly provided respectively bicyclomycin and equipment for toeprinting experiments. Authors would like also to thank Laura Monlezun and Tina Wang for proofreading the manuscript.

AUTHOR CONTRIBUTIONS

F.O. performed the first experiments that initiated the project. C.R.F. performed most of the experiments. S.N. performed northern blotting experiments. C.R.F. prepared the cryo-EM sample. H.S. prepared cryo-EM grids and imaged them. C.A.I. and Y.H. processed cryo-EM data. C.R.F and E.C.L. reconstructed the atomic model. G.B. initiated the project and designed the research program with Y.H. C.R.F. and G.B. wrote the paper with input from all authors.

DECLARATION OF INTERESTS

The authors declare no competing interests. Requests for materials should be addressed to G.B. (boel@ibpc.fr).

498 **MAIN FIGURE TITLES AND LEGENDS**

499 **Figure 1. Translation factor MsrD alleviates erythromycin effects upon translation *in***
500 ***vivo*.** (a) Organization of the *mefA/msrD* macrolide resistance operon. In presence of ERY,
501 ribosomes stall during translation of *mefAL* leading to transcription anti-attenuation, both *mefA*
502 and *msrD* being then transcribed. Similar mechanism occurs during translation of *msrDL*,
503 which regulates transcription of *msrD* only. (b) Sequence alignment of various *msr* homologs
504 visualized with Jalview according to percentage of identity. Positions of tested mutations are
505 highlighted in red and indicated by arrows. Main features of ABC-F proteins are indicated on
506 the schematic. Genebank accession numbers are indicated between brackets. See also
507 Supplementary Fig. 1b. (c and d) Polyribosomes analysis and western blotting of *E. coli* DB10
508 expressing a control (pBAD-*Control*), $msrD_{WT}$ (pBAD-$msrD_{WT}$), $msrD_{EQ2}$ (pBAD-$msrD_{EQ2}$),
509 $msrD_{E125Q}$ (pBAD- $msrD_{E125Q}$) or $msrD_{E434Q}$ (pBAD- $msrD_{E434Q}$) untreated or treated for 1 h with
510 25 µM ERY during mid-log phase. "L" stands for total lysate. See also Supplementary fig. 1c
511 and 1d and Methods. (e to g) Relative growth of *E. coli* DB10 expressing *msrD* variants in
512 presence of ERY after 24 h. Optical densities were normalized relative to optical densities of
513 *E. coli* DB10 pBAD-*Control* grown in the absence of ERY. Error bars represent mean ± s.d. for
514 triplicate experiments. See also supplementary Table 1.

515

516 **Figure 2. Erythromycin-dependent transcriptional attenuation regulates *msrD***
517 **expression.** (a) ERY-dependent induction of $msrD_{(1\text{-}3)}$:*yfp*. Fluorescent reporters shown on
518 schematics have been introduced in *E. coli* DB10 and grew in presence of 1 mM IPTG and
519 increasing sublethal ERY concentrations during 17 h. Fluorescence has been plotted against
520 OD_{600}, error bars for both axes represent mean ± s.d. for triplicate experiments. (b) Northern
521 analysis of *msrD* transcript. RNAs were extracted before adding or not 1 mM IPTG ($T_{0'}$), 10
522 min after adding IPTG ($T_{10'}$), and 5, 15, 30, 60, 120 min after adding or not 100 nM ERY.
523 Location of probe in $msrD_{(1\text{-}3)}$:*yfp* 3' UTR is shown on the schematic. The presence of a second
524 band was also observed but we hypothesized that it was abortive transcript resulting from the
525 construct insofar as its presence correlates with induction by IPTG and ERY, and is no longer
526 detectable using other probes (data not shown). Note the presence of leaky transcription in
527 absence of IPTG, that is slightly amplified in presence of ERY. (c) Deletion of the intrinsic
528 terminator between *msrDL* and $msrD_{(1\text{-}3)}$:*yfp* leads to a constitutive induction in absence of
529 ERY. Error bars for both axes represent mean ± s.d. for triplicate experiments.

530

531 **Figure 3. MsrDL is a macrolide-sensing nascent chain that stalls the ribosome.** (a)
532 Toeprinting assay of *msrDL* in the absence (-) or in the presence of 50 µM of various macrolide
533 antibiotics. White arrow indicates initiation codon. Black arrows indicate ribosome stalling, with
534 M6 codon in the P site. Chemical structure of antibiotics is shown, C3 cladinose sugar of ERY

535 and AZI being highlighted. See also Supplementary fig. 3. (b) *In vivo* induction of *msrD*$_{(1:3)}$:*yfp*
536 by various PTC/NPET targeting antibiotics. Bacteria containing pMMB-*msrDL*-*msrD*$_{(1:3)}$:*yfp*
537 were grown during 17 h in presence of 1 mM IPTG, in the absence (grey histograms) or in the
538 presence of 50 nM antibiotics (red histograms). Error bars represent mean ± s.d. for triplicate
539 experiments. (c) Toeprinting assay depleted of release factors was performed in the absence
540 of ribosome (line 1), in presence of 50 µM RTP to assess start codon (line 2), without or with
541 50 µM ERY (line 3 and 4), without or with 50 µM ERY then supplemented with 100 µM
542 puromycin (line 5 and 6), without or with 50 µM ERY in presence of RF1/RF2/RF3 (line 7 and
543 8). The schematic indicates position of toeprint signal on the synthetic mRNA, P site codon of
544 MsrDL-SRC is underlined. See also Supplementary fig. 3. (d) Effects of *msrDL* variants on the
545 expression of *msrD*$_{(1:3)}$:*yfp*. Bacteria were grown during 17 h in presence of 1 mM IPTG, in the
546 absence (grey histograms) or in the presence of 100 nM ERY (red histograms). Error bars
547 represent mean ± s.d. for triplicate experiments, square boxes show fold of induction. (e)
548 Toeprinting assay performed on the MsrDL$_{7A\text{-}iso}$ construct in absence or presence of ERY.
549 Addition of a sense codon after M6 codon leads to translational arrest with M6 codon in the P
550 site (grey arrows) and A7 codon in the A site in presence of ERY. A faint toeprint is also
551 observed with A7 codon in the P site (black arrows) and the stop codon in the A site.
552
553 **Figure 4. Structure of MsrDL-SRC.** (a) Transverse section of the cryo-EM map showing the
554 30S (grey) and 50S (white) ribosomal subunits, mRNA (purple), ERY (red) and MsrDL-NC
555 (gold) bound to P-site tRNA^{Met} (beige). (b) Close-up of MsrDL-NC within ribosomal tunnel
556 showing experimental density and modelled structure, colored as Fig. 4A while 23S rRNA
557 nucleotides are shown in light grey. (c and d) Presence of MsrDL residue Y2 displace
558 nucleotide U2584 out of its position when compared to RF1- (PDB 5J30, light blue) and RF2-
559 containing (PDB 5CZP, blue) termination complex, thus forming a π-stacking with G2583 [66].
560 (e) Conformation of U2584 and U2585 prevent productive accommodation of RF1 (PDB 5J30,
561 light blue) and RF2 (PDB 5CZP, blue) while catalytic methylated glutamine would clash with
562 MsrDL residue F5[66]. (f) PTC in MsrDL-SRC (light grey) is stabilized in an uninduced state (PDB
563 1VQ6, pink) rather than in an induced state (PDB 1VQN, green) as U2585 is pushed back by
564 MsrDL residue Y2[67]. (g to i) Molecular basis for C3 cladinose sugar recognition by MsrDL.
565 Residue L3 is at proximity of cladinose sugar while residue I4 is at proximity of desosamine
566 sugar. TEL lacking cladinose sugar and failing to form MsrDL-SRC has been aligned (PDB
567 4V7S) [79]. (j) Presence of residue I4 avoids rotation of A2062 to form an Hoogsteen base pairing
568 with m^{2}A2503 as it is the case for ErmCL-SRC (PDB 3J7Z, green)[12]. Light blue dashed lines
569 indicate hydrogen bonds formed by Hoogsteen base pairing. For the whole figure, structures
570 were aligned on domain V of 23S rRNA. Spheres represent van der Waals radii.
571

572 **Figure 5. MsrDL engages in a conserved crevice at the NPET entrance.** (a) Secondary
573 structure of the *E. coli* 23S rRNA domain V showing location of the proximal crevice at the
574 base of h93. For the whole figure, nucleotides delimitating proximal crevice are shown in red.
575 (b and c) Comparison of MsrDL path (gold) with ERY-dependent leader peptides ErmBL (PDB
576 5JTE, blue), ErmCL (PDB 3J7Z, green), ErmDL (PDB 7NSO, teal) as well as L-ornithine-
577 sensing SpeFL (PDB 6TC3, pink) and L-tryptophan-sensing TnaC(R23F) (PDB 7O1A,
578 purple)[12–16]. See also Supplementary fig. 5a to 5e**.** (d) Proximal crevice in domain V is
579 conserved from bacteria to human (MsrDL-SRC, grey; *S. aureus* PDB 6YEF, light green; *H.*
580 *sapiens* 55S mitoribosome PDB 7A5F, light blue; *H. sapiens* 80S ribosome PDB 6OLI, marine
581 blue)[80–82]. See also Supplementary fig. 5g and 5h. For the whole figure, atomic model of MsrDL
582 is shown with its experimental density. Structures were aligned on domain V of 23S rRNA.
583
584 **Figure 6. MsrD negatively regulates its own synthesis upon erythromycin exposure.** (a)
585 Effects of MsrD variants on MsrDL. *E. coli* DB10 containing pMMB-*msrDL-msrD*(1-3)*:yfp* and
586 expressing various *msrD* mutants were grown in presence of 0.2 % L-Arabinose, 1 mM IPTG
587 and 300 nM ERY, both OD_{600} and fluorescence being recorded over 24 h. Fluorescence has
588 been plotted against OD_{600}, error bars for both axes represent mean ± s.d. for triplicate
589 experiments. Color code is same as Fig. 1e to 1g. Light green rectangle indicates bacterial
590 growth over control plasmid. (b) Model of MsrD regulating its own expression and providing
591 antibiotic resistance. Presence of a NusG-dependent pause site may stall the RNAP and
592 provides explanation why the system works in bacteria where transcription and translation are
593 not so tightly coupled. In absence of ERY, RNAP drops off at Rho-independent transcription
594 terminator. In presence of ERY, the ribosome following the RNAP (presumably paused) stalls
595 and unwinds the terminator leading to *msrD* transcription. Once translated, MsrD negatively
596 regulates its own expression on one side, and provides antibiotic resistance on the other side.
597 ATP-bound MsrD recognizes ERY-stalled ribosome and may either expel the antibiotic or
598 dissociate the ribosome, ATP site II being active. Activity in ATP site I may lead to MsrD
599 dissociation and recycling.

600 **MAIN TABLE TITLES AND LEGENDS**

601 **Table 1. Minimum inhibitory concentration (MIC) and half maximal inhibitory**
602 **concentration (IC_{50}) of *E. coli* DB10 expressing *msrD* in presence of ribosome-targeting**
603 **antibiotics.** See Methods for experimental details.

604

605

	pBAD-*Control*		pBAD-*msrD*$_{WT}$	
Antibiotic	**MIC (µM)**	**IC_{50} (µM)**	**MIC (µM)**	**IC_{50} (µM)**
Erythromycin	2	0,179 ± 0,007	16	4,592 ± 0,582
Azithromycin	0.25	0,046 ± 0,002	2	0,953 ± 0,053
Telithromycin	1	0,086 ± 0,008	2	0,714 ± 0,066
Tylosin	4	1,649 ± 0,151	4	1,672 ± 0,103
Spiramycin	2	0,758 ± 0,063	2	0,81 ± 0,078
Lincomycin	32	12,61 ± 2,154	32	12,62 ± 1,27
Linezolid	32	13,62 ± 2,064	32	13,41 ± 1,137
Retapamulin	1	0,071 ± 0,004	1	0,075 ± 0,007

606 **METHOD DETAILS**

607 **Construction of plasmids**

608 Strains and plasmids used in this study are listed in Supplementary Table 3. Oligonucleotides
609 are listed in Supplementary Table 4. For the whole study, the considered reference sequence
610 for *mefA/msrD* macrolide resistance operon was a Tn916-type transposon inserted in
611 *Streptococcus pneumoniae* strain 23771 genome (Genbank accession number
612 FR671415.1)[83]. Plasmids pBAD-*Control* and pBAD-$msrD_{WT}$ containing a C-terminal
613 hexahistidine tag (originally referred as pBAD33 and pVN50) were kindly retrieved from Olivier
614 Chesneau at Institut Pasteur (Paris, France)[24]. Both *mefA/msrD* macrolide resistance operon
615 and pBAD-$msrD_{WT}$ encode the same protein MsrD (Uniprot accession number A0A496M710).
616

617 **pBAD plasmids**. Those plasmids allow a tight and stringent expression control via catabolite
618 repression, interest gene being repressed in presence of 0.4 % (w/v) β-D-Glucose and induced
619 in presence of 0.2 % (w/v) L-Arabinose. Transformed clones were selected with 20 $\mu g.ml^{-1}$
620 chloramphenicol. In this study, all *msrD* mutants contain a C-terminal hexahistidine tag.
621 Catalytic mutant $msrD_{EQ2}$ was generated by amplifying pBAD-$msrD_{WT}$ with primer pairs 5/6 and
622 7/8, both fragments being assembled with NEBuilder HiFi DNA Assembly Master Mix (New
623 England Biolabs). Catalytic mutants $msrD_{E125Q}$, $msrD_{E434Q}$ were generated via quickchange
624 mutagenesis with primers pairs 9/10 and 11/12. Mutants $msrD_{\Delta Loop}$ and $msrD_{\Delta PtlM}$ were
625 generated based on phylogenetic alignments by deleting residues between K216/K254 and
626 E189/A274 respectively, a three-glycine linker being added to allow flexibility, via quickchange
627 mutagenesis using primer pairs 13/14 and 15/16. Variants $msrD_{R241A}$, $msrD_{L242A}$, $msrD_{H244A}$,
628 $msrD_{H244W}$ were generated via fusion PCR by amplifying $msrD_{WT}$ with primers pairs 1/18, 1/20,
629 1/22, 1/24 and 2/17, 2/19, 2/21, 2/23 respectively. Backbone was amplified with primer pair
630 3/4 and fragments were assembled with NEBuilder HiFi DNA Assembly Master Mix (New
631 England Biolabs).

632 **pMMB plasmids**. All pMMB constructs originated from a low copy IPTG-inducible plasmid
633 pMMB67EH-*yfp*, consisting in original pMMB67EH[45] containing optimized *venus-yfp*
634 enhancing its translation under the control of P_{tac} promoter (manuscript in preparation).
635 Transformed clones were selected with 100 $\mu g.ml^{-1}$ ampicillin. To test *msrDL* functions *in vivo*,
636 several fluorescent reporter genes have been designed. First, pMMB67EH-*yfp* native P_{tac}
637 promoter was replaced by $P_{LlacO-1}$ promoter as previously described[46]:
638 5'- ATAAATGTGAGCGGATAACATTGACATTGTGAGCGGATAACAAGATACTGAGCAC**A** -
639 3' (lac operators, shaded grey; transcription start, bold). This IPTG-inducible promoter allows
640 a tight and stringent transcription regulation compared to P_{tac} promoter, insofar as no regulatory
641 element is found in the 5' UTR. Promoter was replaced by amplifying pMMB67EH-*yfp* with
642 primer pairs 25/26, PCR fragment being then re-circularized via NEBuilder HiFi DNA Assembly

643 Master Mix (New England Biolabs). The resulting plasmid was named pMMBpLlacO-1-67EH-
644 *yfp*. Plasmid pMMB-*msrDL*-*msrD*$_{(1-3)}$*:yfp* has been designed by introducing the sequence
645 spanning from the first nucleotide downstream *mefA* stop codon to *msrD* three first codons
646 fused to *yfp*. The introduced sequence is as follows: 5'-
647 ACAATATT**GGAGGA**ATATTTATGTATCTTATTTTCATGTAACTCTTCCTGCTAAAATCGCA
648 GGGTTTTCCCTGCATACAAGCAAATGAAAGCATGCGATTATAGACA**GGAGGA**AATGTTA
649 TGGAATTA-3' (RBS, bold; *msrDL*, shaded grey, *msrD* three first codons are underlined). To
650 clone such construct, *yfp* gene was amplified from pMMB67EH-*yfp* with primer pairs 27/29
651 then with 28/29 to generate the insert, backbone was amplified with primer pair 30/31 using
652 pMMBpLlacO-1-67EH-*yfp* as matrix, both fragments being then assembled with NEBuilder
653 HiFi DNA Assembly Master Mix (New England Biolabs). Plasmid pMMB-*control* was built by
654 removing the *msrDL*-*msrD*$_{(1-3)}$*:yfp* cassette via quickchange mutagenesis using primer pair
655 32/33, the resulting construction containing only the $P_{LlacO-1}$ promoter followed by the plasmid
656 endogenous *rrnB* transcription terminator. Plasmid pMMB-*msrDL*$_{(no_term)}$-*msrD*$_{(1-3)}$*:yfp (*where
657 the RIT between *msrDL* and *msrD* is deleted) was generated by amplifying pMMB-*msrDL*-
658 *msrD*$_{(1-3)}$*:yfp* with primer pair 34/35, PCR fragment being then re-circularized via NEBuilder
659 HiFi DNA Assembly Master Mix (New England Biolabs). The various *msrDL* mutants were
660 cloned via quickchange mutagenesis by amplifying pMMB-*msrDL*-*msrD*$_{(1-3)}$*:yfp* with primers
661 36 to 51. Plasmid pMMB-*msrDL*$_{(MYLIFMA-isocodons)}$-*msrD*$_{(1-3)}$:*yfp* was generated by replacing
662 *msrDL*$_{WT}$ sequence (ATGTATCTTATTTTCATGTAA) by a recoded sequence
663 (ATGTACCTGATCTTCATGGCCTAA) using isocodons and introducing an extra alanine
664 codon (7A codon) before stop codon. Sequence was recoded using isocodons because
665 mutating the WT sequence introduced a new promoter. To do so, pMMB-*msrDL*-*msrD*$_{(1-3)}$*:yfp*
666 was amplified with primer pair 52/53, PCR fragment being then re-circularized via NEBuilder
667 HiFi DNA Assembly Master Mix (New England Biolabs). Recoded sequence without the 7A
668 codon (ATGTACCTGATCTTCATGTAA) was generated via quickchange mutagenesis by
669 amplifying pMMB-*msrDL*$_{(MYLIFMA-isocodons)}$-*msrD*$_{(1-3)}$:*yfp* with primer pair 54/55, leading to plasmid
670 pMMB-*msrDL*$_{(WT-isocodons)}$-*msrD*$_{(1-3)}$*:yfp.*
671

672 **Antibiotic susceptibility testing, MIC and IC50 determination**

673 A saturated preculture of *E. coli* DB10 transformed with pBAD plasmid was grown overnight at
674 37 °C under vigorous shaking in Luria-Bertani Miller broth (LB), 20 µg.ml^{-1} chloramphenicol
675 and supplemented with 0.4 % (w/v) β-D-Glucose. Antibiotic susceptibility testing assay was
676 performed in Mueller-Hinton broth (MH, Sigma Aldrich), antibiotics being diluted via serial
677 dilutions. A 96-wells flat-bottom plate (Flacon) was filled with a final volume per well of 200 µl,
678 containing 20 µg.ml^{-1} chloramphenicol and 0.2 % (w/v) L-Arabinose and antibiotic to test. Wells
679 were inoculated at OD_{600} ~0.03-0.04 prior to addition of 60 µl mineral oil (Sigma Aldrich)

680 avoiding evaporation but not oxygen diffusion. Plates were therefore incubated for 24 h in
681 CLARIOstar Plus plate reader (BMG Labtech) at 37 °C with 600 rpm double-orbital shaking,
682 OD_{600} being measured each 30 min. Optical densities at 24 h were then normalized relative to
683 optical densities of *E. coli* DB10 pBAD-*Control* grown in the absence of antibiotic in Prism
684 7(GraphPad). MIC was determined as absence of growth compared to blank, IC50 was
685 calculated in Prism using equation Y=Bottom + (Top-
686 Bottom)/(1 + ((X^HillSlope)/(IC50^HillSlope))) and the standard deviation was calculated by
687 multiplying standard error by square root of n (n being at least 3 replicates). To generate
688 curves, for bacteria grown in absence of antibiotic (0 µM), since coordinates are plotted as
689 logarithms and since log(0) is undefined, this point has been approximated 2 log units below
690 the lowest tested value (*i.e.* 0.0625 µM) consistently with Prism user guide[84]. Curve fitting was
691 performed with non-linear fitting function "log(inhibitor) vs. response -- Variable slope" using
692 Y=Bottom + (Top-Bottom)/(1+10^((LogIC50-X)*HillSlope)). Both equations gave strictly the
693 same result for IC_{50}.
694
695 ***In vivo* induction assay**
696 A saturated preculture of *E. coli* DB10 transformed with pMMB plasmid was grown overnight
697 at 37 °C under vigorous shaking in LB with 100 µg.ml^{-1} ampicillin. For bacteria double-
698 transformed with pMMB and pBAD plasmids, media was also supplemented with 20 µg.ml^{-1}
699 chloramphenicol and supplemented with 0.4 % (w/v) β-D-Glucose. *In vivo* induction assay was
700 performed in Mueller-Hinton broth (MH, Sigma Aldrich). A 96-wells flat-bottom plate (Flacon)
701 was filled with a final volume per well of 200 µl, containing 100 µg.ml^{-1} ampicillin, 1 mM
702 Isopropyl β-D-1-thiogalactopyranoside (IPTG). Growth medium was supplemented with 20
703 µg.ml^{-1} chloramphenicol and 0.2 % (w/v) L-Arabinose if pBAD plasmid is present. Induction of
704 fluorescent reporters being antibiotic-dependent, growth media were supplemented with
705 required antibiotic accordingly. Plates were therefore incubated in CLARIOstar Plus plate
706 reader (BMG labtech) at 37 °C with 600 rpm double-orbital shaking up to 24 h, OD_{600} and
707 fluorescence (excitation: 497-15 nm, emission: 540-20 nm, gain 1600) being measured each
708 30 min.
709
710 **Polyribosomes fractionation**
711 Saturated precultures of *E. coli* DB10 transformed with pBAD-*control*, pBAD-$msrD_{WT}$, pBAD-
712 $msrD_{EQ2}$, pBAD-$msrD_{E125Q}$ or pBAD-$msrD_{E434Q}$ were grown overnight at 37 °C under vigorous
713 shaking in LB, 20 µg.ml^{-1} chloramphenicol, 0.4 % (w/v) β-D-Glucose. Growth media (MH, 20
714 µg.ml^{-1} chloramphenicol, 0.2 % (w/v) L-Arabinose) was inoculated at OD_{600}=0.05 with
715 normalized precultures, and cells were grown at 37 °C and 180 rpm. When OD_{600}=0.5 was
716 reached, cultures were divided in two and one half was treated with a 25 µM erythromycin.

717 Cultures were then incubated 1 hour at 37 °C and 180 rpm before harvesting. Cultures were
718 chilled and cells were harvested by centrifuging 10 min at 8 000 rpm, 4 °C. Supernatant was
719 discarded and cells were resuspended in 350 µl of lysis buffer (20 mM Tris pH 8, 20 mM $MgCl_2$,
720 100 mM NH_4(OAc), 2 mM β-mercaptoethanol, 1 $mg.ml^{-1}$ lysozyme) and transferred in
721 microtubes. Then, 30 µl of sodium deoxycholate 10 % (w/v) was added and cells were
722 mechanically lysed by 3 rounds of freezing-thawing. Lysates were clarified by centrifuging 20
723 min at 18 000 xg, 4 °C and total RNAs were quantified. Finally, 500 µg of total RNAs were
724 loaded onto 10-40 % (w/v) sucrose gradients (20 mM Tris pH 8, 20 mM $MgCl_2$, 100 mM
725 NH_4(OAc), 2 mM β-mercaptoethanol) and centrifuged 2 h at 40 000 rpm, 4 °C in SW41 rotor
726 (Beckman Coulter). Samples were fractionated and collected using Biocomp Piston Gradient
727 Fractionator (BioComp Instruments), absorbance being measured at 254 nm.
728
729 **Immunoblotting**
730 Fractions of 400 µl were precipitated in ice-cold absolute ethanol (1 volume of sample, 3
731 volumes of ethanol) overnight at -20 °C. Samples were then centrifuged 45 min at 18 000 xg,
732 4 °C. Supernatant was removed and samples were vacuum-dried. Pellets were resuspended
733 in 33.3 µl 1X Laemmli buffer, 10 µl being loaded on 12.5 % acrylamide SDS-PAGE gels.
734 Concerning total lysates, 10 µg of normalized total RNAs were loaded as control. Gels were
735 resolved by migrating at 0.04 A and then applied on Immun-Blot PVDF membrane (Bio-Rad)
736 that had been activated in absolute ethanol then washed in electro-transfer buffer (25 mM Tris
737 base, 192 mM glycine, 0.1 % (w/v) SDS, 10 % (v/v) absolute ethanol). Proteins were electro-
738 transferred at 100 V during 1 h. Membranes were blocked by incubating 1 h in 1X PBS
739 supplemented with 0.5 % nonfat dry milk then washed with 1X PBS. C-term His-tagged $MsrD_{WT}$
740 and $MsrD_{EQ2}$ were detected using anti-6xHis-tag primary antibody (Covalab, 1:2 000 dilution
741 in 1X PBS, 0.1 % Tween-20) combined with anti-mouse-HRP secondary antibody (Covalab,
742 1:20 000 dilution in 1X PBS, 0.1 % Tween-20). Immunoblots were revealed by performing an
743 ECL detection using Clarity Western ECL Substrate (Bio-Rad) and imaged with Li-Cor
744 Odyssey FC imaging system (Li-Cor).
745
746 **Preparation of *E. coli* DB10 ribosomes**
747 An overnight saturated *E. coli* DB10 preculture was used to inoculate growth medium (LB,
748 dilution 1:100) and cells were grown at 37 °C and 180 rpm. When OD_{600}=0.5, cells were
749 washed and harvested by two centrifugations during 20 min, 5 000 xg at 4°C followed by
750 resuspensions in Buffer A (20 mM Tris pH 7.4, 10 mM Mg(OAc), 100 mM NH_4(OAc), 0.5 mM
751 EDTA). Pellets were resuspended in Buffer A supplemented with 6 mM β-mercaptoethanol,
752 10 $mg.ml^{-1}$ lysozyme, 0.001 % (v/v) protease inhibitor cocktail (Sigma Aldrich) and lysed three
753 times at 2.5 kBar using a cell disrupter (Constant Systems Limited). Lysate was clarified by

754 two centrifugations during 15 min, 22 000 xg at 4°C then spun for 20 h, 34 700 rpm at 4 °C in
755 a Type 70 Ti rotor (Beckmann Coulter) through a 37.7 % (w/v) sucrose cushion in Buffer B (20
756 mM Tris pH 7.4, 10 mM Mg(OAc), 500 mM NH_4(OAc), 0.5 mM EDTA, 6 mM β-
757 mercaptoethanol). Sucrose cushions were decanted and ribosome pellets resuspended in
758 Buffer C (20 mM Tris pH 7.4, 7.5 mM Mg(OAc), 60 mM NH_4(OAc), 0.5 mM EDTA, 6 mM β-
759 mercaptoethanol). Finally, 12 mg of ribosomes were loaded onto 10-40 % (w/v) sucrose
760 gradients in Buffer C and centrifuged 18 h at 20 000 rpm, 4 °C in SW28 rotor (Beckman
761 Coulter). Gradients were fractionated using Biocomp Piston Gradient Fractionator (BioComp
762 Instruments), absorbance being measured at 254 nm. Fractions containing 70S ribosomes
763 were pooled, washed and concentrated in Amicon 50k (Merckmillipore) using Buffer C.
764 Ribosomes concentration was adjusted to 18-20 µM, then aliquoted and flash frozen in liquid
765 nitrogen.
766
767 **RNA extraction and northern blotting**
768 Total RNA extraction was realized using the RNAsnap method as previously described[85]. In
769 brief, a preculture of *E. coli* DB10 containing pMMB-*msrDL-msrD*$_{(1-3)}$*:yfp* was grown overnight
770 at 37 °C under vigorous shaking in LB supplemented with 100 µg.ml^{-1} ampicillin. Growth
771 medium (MH, 100 µg.ml^{-1} ampicillin) was inoculated at OD_{600}=0.05, and cells were grown at
772 37 °C and 180 rpm. When OD_{600}=0.5, cells were treated (or not) with 1 mM IPTG during 10
773 min, then treated (or not) with 100 nM erythromycin. Samples of 2 ml were collected ($T_{0'}$ =
774 before IPTG was added, $T_{10'}$= 10 min after IPTG was added, and 5 min, 15 min, 30 min, 60
775 min and 120 min after erythromycin was added), then spun during 1 min at 15 000 rpm. Growth
776 media was removed and cells were resuspended in 100 µl RNAsnap buffer (95 % (v/v)
777 formamide, 18 mM EDTA, 0.025 % (v/v) SDS, 1 % (v/v) β-mercaptoethanol). Samples were
778 heated for 10 min at 95 °C then clarified by centrifuging 10 min, at 16 000 rpm at 16 °C. For
779 northern blotting analysis, 6 µg of total RNAs were resolved on a 1 % (w/v) agarose gel then
780 transferred onto Amersham Hybond-N+ Membrane (GE Healthcare) by capillary transfer.
781 Radioactive probe was prepared using 40 pmol of primer 59 and 5'-labelled with 10 U of T4
782 Polynucleotide Kinase (New England Biolabs) and [γ^{32}P]ATP (150 µCi). Probe was hybridized
783 overnight at 42 °C using ULTRAhyb-Oligo hybridization buffer (Thermo Fisher Scientific).
784 Membrane was washed three times at 42 °C during 15 min (once in 2x SSC + 0.1 % (v/v) SDS,
785 once in 1x SSC + 0.1 % (v/v) SDS and finally in 0.1x SSC + 0.1 % (v/v) SDS). Radioactive
786 signal was visualized by exposing 4 h a Storage Phosphor Screen BAS-IP MS 2040 (Fujifilm)
787 then imaged with a Typhoon FLA 9500 (GE Healthcare).
788

789 ***In vitro* transcription**

790 *In vitro* transcription was carried out in T7 RiboMAX Large Scale RNA Production System kit
791 (Promega) according to manufacturer instructions. Briefly, to generate DNA matrix
792 (Supplementary Table 5), T7 promoter (5'-GCGAATTAATACGACTCACTATAGGG-3') was
793 added by PCR using primers pair 56/57 (Supplementary Table 4) and pMMB plasmids as
794 templates. Transcription reactions were incubated 4 h at 37 °C and transcripts were purified
795 with TRIzol Reagent (Thermo Fisher Scientific) and Direct-zol RNA Miniprep kit (Zymo
796 Research), samples being eluted in THE Ambion RNA Storage Solution (Thermo Fisher
797 Scientific). Final concentration was adjusted to 5 pmol.μl^{-1}.

798

799 **Toeprinting assay**

800 Position of stalled ribosomes on mRNA was determined by toeprinting assay, slightly adapted
801 from previously described methods[15,86]. *In vitro* translation reactions were performed using
802 PURExpress ΔRF123 kit and PURExpress ΔRibosome (New England Biolabs) according to
803 manufacturer instructions. Briefly, prior to *in vitro* translation reactions, 0.5 µl of 500 µM ligand
804 (e.g. erythromycin etc) was dried in a micro-centrifuge tube, using a SpeedVac vacuum
805 concentrator (Thermo Fisher Scientific), final concentration being 50 µM once resuspended in
806 a 5 µl reaction. Reactions were incubated during 15 min at 37 °C using 5 pmol of RNA
807 templates (generated as described above) and 3.3 µM of purified *E. coli* DB10 ribosomes.
808 When needed, samples were treated with 100 µM final puromycin and incubated 3 min more.
809 Immediately, 2 pmol of CY5-labelled primer 58 complementary to NV1 sequence [20] was added
810 and incubated for 5 min at 37 °C. For each reaction, reverse transcription was performed with
811 0.5 µl (corresponding to 5 U) of Avian Myeloblastosis Virus Reverse Transcriptase (Promega),
812 0.1 µl dNTP mix (10 mM), 0.4 µl Pure System Buffer (5 mM K-phosphate pH 7.3, 9 mM
813 Mg(OAc), 95 mM K-glutamate, 5 mM NH_4Cl, 0.5 mM $CaCl_2$, 1 mM spermidine, 8 mM
814 putrescine, 1 mM DTT) and incubated 20 min at 37 °C. Reactions were quenched with 1 µl
815 NaOH 5 M and incubated 15 min at 37 °C. Alkali were therefore neutralized by adding 0.7 µl
816 HCl 25% immediately supplemented with 20 µl toe-printing resuspension buffer (300 mM
817 Na(OAc) pH 5.5, 5 mM EDTA, 0.5% (v/v) SDS). Finally, cDNAs were purified using QIAquick
818 Nucleotide Removal kit (Qiagen), vacuum dried and resuspended in 6 µl formamide dye (95%
819 (v/v) formamide, 20 mM EDTA, 0.25% (w/v) bromophenol blue). Sanger sequencing was
820 performed on DNA matrix used for *in vitro* transcription. Briefly, each 20 µl reaction contained
821 7.5 nM DNA matrix, 75 nM CY5-labelled primer 58, 40 µM of each dNTPs, 0.025 U Taq Pol
822 (New England Biolabds), 1x Thermo Pol Buffer (New England Biolabs) and corresponding
823 ddNTPs (625 µM ddCTP/ddTTP/ddATP or 50 µM ddGTP). After PCR, 20 µl formamide dye
824 was added to each sequencing reaction. Samples were denatured 3 min at 80 °C, then 5 µl of

825 sequencing reaction and 1.5 µl of toe-printing reaction were loaded on a 6% acrylamide/bis-
826 acrylamide (19:1) sequencing gel containing 8 M urea. Gel was resolved by migrating 90 min
827 at 50 W, then imaged using a Typhoon FLA 9500 (GE Healthcare Life Sciences) using CY5
828 mode, LPR Ch.2 filter and 635 nm laser.
829

830 **Preparation of MsrDL-SRC**

831 A DNA matrix (Supplementary Table 5) was prepared with CloneAmp HiFi PCR Premix
832 (Takara) using primer pair 56/60 (Supplementary Table 4) and plasmid pMMB-*msrDL*-
833 *msrD*$_{(1-3)}$*:yfp* as matrix. The corresponding mRNA was generated as described above. The
834 complete sequence of MsrDL-SRC mRNA is:

835 5'- GGAGCGGAUAACAAGAUACUGAGCACAACAAUAUU**GGAGG**AAUAUUUAUGUAU
836 CUUAUUUUCAUGUAACUCUUCCUGCUAAAAUCGCAGGGUUUUCCCUGC -3' (RBS, bold;
837 *msrDL*, shaded grey; the ATG codon in the P site of stalled ribosomes is underlined). Prior to
838 *in vitro* translation reaction, 1 µl of 500 µM erythromycin (50 µM final concentration once
839 resuspended in 10 µl) has been dried in a micro-centrifuge tube, using a SpeedVac vacuum
840 concentrator (Thermo Fisher Scientific). Dried erythromycin has been resuspended in a 10 µl
841 *in vitro* translation reaction carried out in PURE*frex* 2.0 kit (Genefrontier), containing 1.83 µM
842 of purified *E. coli* DB10 ribosomes and 3.6 µM mRNA (molar ratio 1:2). The reaction has been
843 incubated for 10 minutes at 37 °C, before adding 100 µM final puromycin, and incubated 3 min
844 more. Reaction was therefore diluted in ribosome purification Buffer C (20 mM Tris pH 7.4, 7.5
845 mM Mg(OAc), 60 mM NH_4(OAc), 0.5 mM EDTA, 6 mM β-mercaptoethanol) to reach a
846 concentration of 150 nM ribosomes. Cryo-EM grids were immediately prepared.
847

848 **Cryo-EM grids preparation**

849 Safematic ccu-010 HV carbon coater was used to coat Quantifoil carbon grids (QF-R2/2-Cu)
850 with a thin carbon layer of approximate thickness of 2nm. Grids were therefore glow discharged
851 for 30 sec at 2 mA. Then, 4 µl of *in vitro* translation reaction diluted to 150 nM were applied,
852 and after a 2 sec blotting (force 5) and 30 sec waiting time, grids were vitrified in liquid ethane
853 using a Vitrobot Mark IV (FEI) set to 4 °C and 100 % humidity.
854

855 **Image acquisition and processing**

856 Data collection was performed on a Talos Arctica instrument (FEI Company) at 200 kV using
857 the EPU software (Thermo Fisher Company) for automated data acquisition. Data were
858 collected at a nominal defocus of -0.5 to -2.7 µm at a magnification of 120,000 X yielding a
859 calibrated pixel size of 1.2 Å. Micrographs were recorded as movie stack on a K2 Summit
860 direct electron detector (Gatan), each movie stack were fractionated into 65 frames for a total

861 exposure of 6.5 sec corresponding to an electron dose of 64 $e^-/Å^2$. MotionCor2 [87] was used for
862 dose weighting, drift and whole-frame motion correction. A dose weighted average image of
863 the whole stack was used to determine the contrast transfer function with the software Gctf[88].
864 Particles were picked using a Laplacian of gaussian function (min diameter 260 Å, max
865 diameter 320 Å). A total of ~254k particles were extracted from a subset of motion-corrected
866 images (1523 micrographs) presenting a resolution equal or better than 4 Å with a box size of
867 360 pixels. The particles were binned three folds for 2D and subsequent 3D classification. After
868 2 rounds of 2D classification in RELION 3[89], ~158k particles were selected and submitted to
869 Relion 3D classification[89]. A class of non-rotated 70S depicting high-resolution features and
870 bearing a tRNA with various occupancies was selected, representing ~104k particles. This
871 class was further 3D-classified with a spherical mask engulfing the tRNAs binding sites
872 (Supplementary Fig. 4b) into 4 classes, thus yielding to P- and E-tRNAs, P-tRNAs only, A- and
873 P-tRNAs and E-tRNAs 70S reconstructions. Only P- and E-tRNAs and P-tRNAs only
874 reconstructions were used for further processing, which represents ~62k particles displaying
875 the same global conformation of the 70S. These particles where re-extracted at the full pixel
876 size (1.2 Å) and refined through the 3D auto-refinement performed in RELION 3[89] resulting in
877 a 3 Å reconstruction (Supplementary Fig. 4c), after CTF-refinement, Bayesian particle
878 polishing and post-processing in RELION 3. In spite of the sufficient local resolution at the
879 vicinity of MsrDL peptide at the PTC (~3Å), residual movements of the 30S around the 50S
880 can be deduced by the lower local resolutions of the head and the body of the 30S. In order to
881 improve their resolution so to derive a complete atomic model of the entire 70S complex, we
882 applied RELION 3 multi-body refinement by defining three bodies; 50S, 30S-head and 30S-
883 body. After completion of the refinement, the reconstructions of the 30S-head, 30S-body and
884 50S reached average resolutions of 3.3, 3.08 and 2.97 Å, respectively. The local resolution
885 (Supplementary Fig. 4b and 4d) was estimated using ResMap[90].
886

887 **Model building and refinement**

888 The atomic model of erythromycin-stalled *Escherichia coli* 70S ribosome with streptococcal
889 MsrDL nascent chain was built into cryo-EM maps using Coot and Phenix[91,92]. Insofar as *E.*
890 *coli* DB10 hasn't been sequenced yet, we assumed that ribosomal proteins and rRNAs were
891 strictly identical to *E. coli* K12. Furthermore, we did not notice any significant features in the
892 map. Structure of SpeFL-SRC in response to L-ornithine was used as initial model (PDB
893 6TC3)[15] and has been fitted in 70S ribosome map EMD-13805. Then, each part of the
894 ribosome (50S, 30S Body and 30S Head) has been individually inspected in the corresponding
895 map (respectively EMD-13806, EMD-13807 and EMD-13808) modified if necessary in Coot.
896 P-site elongator tRNA $_{Met}$tRNA^{Met} was modeled *de novo* based on *E. coli* K12 MG1655 *metT*
897 gene, posttranscriptional modifications were added consistently with Modomics database[93]

898 (http://genesilico.pl/modomics/). E-site tRNA $_{Phe}$tRNA^{Phe} was derived from crystal structure of
899 phenylalanine tRNA from *E. coli* (PDB 6Y3G) with minor adjustments[94]. ERY, MsrDL leader
900 peptide and mRNA were modeled *de novo* in Coot. Final model was refined in map EMD-
901 13805 using Phenix[92].
902
903 **Figure preparation**
904 Growth curves, histograms and polyribosomes profiles were generated using GraphPad Prism
905 7 (GraphPad). Sequence alignments were visualized with JalView[95]. Western blotting, northern
906 blotting and toe-printing gels were analyzed using Fiji[96]. Figures depicting molecular structures
907 or electronic density maps were prepared using PyMOL Molecular Graphics System, Chimera
908 and ChimeraX[97,98].
909
910 **Quantification and statistical analysis**
911 Statistical details can be found in the figure legends. Statistical significance was assessed
912 using unpaired t-Test function in Prism 7 (GraphPad).
913
914 **Data and software availability**
915 Cryo-EM map of erythromycin-stalled *Escherichia coli* 70S ribosome with streptococcal MsrDL
916 nascent chain has been deposited at the Electron Microscopy Data Bank (EMDB) with
917 accession code EMD-13805, as well as 50S, 30S Body and 30S Head maps obtained after
918 multibody refinement with accession code EMD-13806, EMD-13807, EMD-13808 respectively.
919 Corresponding atomic model has been deposited in the Protein Data Bank (PDB) with
920 accession code 7Q4K.
921

REFERENCES

1. Crowe-McAuliffe, C. *et al.* Structural basis for antibiotic resistance mediated by the Bacillus subtilis ABCF ATPase VmlR. *PNAS* **115**, 8978–8983 (2018).
2. Crowe-McAuliffe, C. *et al.* Structural basis of ABCF-mediated resistance to pleuromutilin, lincosamide, and streptogramin A antibiotics in Gram-positive pathogens. *Nat Commun* **12**, 3577 (2021).
3. Crowe-McAuliffe, C. *et al.* Structural basis for PoxtA-mediated resistance to phenicol and oxazolidinone antibiotics. *Nat Commun* **13**, 1860 (2022).
4. Lenart, J., Vimberg, V., Vesela, L., Janata, J. & Balikova Novotna, G. Detailed Mutational Analysis of Vga(A) Interdomain Linker: Implication for Antibiotic Resistance Specificity and Mechanism. *Antimicrob Agents Chemother* **59**, 1360–1364 (2015).
5. Mohamad, M. *et al.* Sal-type ABC-F proteins: intrinsic and common mediators of pleuromutilin resistance by target protection in staphylococci. *Nucleic Acids Research* **50**, 2128–2142 (2022).
6. Sharkey, L. K. R., Edwards, T. A. & O'Neill, A. J. ABC-F Proteins Mediate Antibiotic Resistance through Ribosomal Protection. *mBio* **7**, (2016).
7. Su, W. *et al.* Ribosome protection by antibiotic resistance ATP-binding cassette protein. *PNAS* **115**, 5157–5162 (2018).
8. Boël, G. *et al.* The ABC-F protein EttA gates ribosome entry into the translation elongation cycle. *Nat Struct Mol Biol* **21**, 143–151 (2014).
9. Chen, B. *et al.* EttA regulates translation by binding the ribosomal E site and restricting ribosome-tRNA dynamics. *Nat Struct Mol Biol* **21**, 152–159 (2014).
10. Fostier, C. R. *et al.* ABC-F translation factors: from antibiotic resistance to immune response. *FEBS Letters* **595**, 675–706 (2021).
11. Ousalem, F., Singh, S., Chesneau, O., Hunt, J. F. & Boël, G. ABC-F proteins in mRNA translation and antibiotic resistance. *Research in Microbiology* **170**, 435–447 (2019).
12. Arenz, S. *et al.* Drug Sensing by the Ribosome Induces Translational Arrest via Active Site Perturbation. *Molecular Cell* **56**, 446–452 (2014).
13. Arenz, S. *et al.* A combined cryo-EM and molecular dynamics approach reveals the mechanism of ErmBL-mediated translation arrest. *Nat Commun* **7**, (2016).
14. Beckert, B. *et al.* Structural and mechanistic basis for translation inhibition by macrolide and ketolide antibiotics. *Nat Commun* **12**, 4466 (2021).
15. Herrero del Valle, A. *et al.* Ornithine capture by a translating ribosome controls bacterial polyamine synthesis. *Nature Microbiology* **5**, 554–561 (2020).
16. van der Stel, A.-X. *et al.* Structural basis for the tryptophan sensitivity of TnaC-mediated ribosome stalling. *Nat Commun* **12**, 5340 (2021).
17. Horinouchi, S. & Weisblum, B. Posttranscriptional modification of mRNA conformation: Mechanism that regulates erythromycin-induced resistance. *PNAS* **77**, 7079–7083 (1980).
18. Ito, K. & Chiba, S. Arrest Peptides: Cis-Acting Modulators of Translation. *Annu. Rev. Biochem.* **82**, 171–202 (2013).
19. Narayanan, C. S. & Dubnau, D. Evidence for the translational attenuation model: ribosome-binding studies and structural analysis with an in vitro run-off transcript of ermC. *Nucleic Acids Res* **13**, 7307–7326 (1985).
20. Vazquez-Laslop, N., Thum, C. & Mankin, A. S. Molecular Mechanism of Drug-Dependent Ribosome Stalling. *Molecular Cell* **30**, 190–202 (2008).

21. Gay, K. & Stephens, D. S. Structure and Dissemination of a Chromosomal Insertion Element Encoding Macrolide Efflux in Streptococcus pneumoniae. *The Journal of Infectious Diseases* **184**, 56–65 (2001).
22. Roberts, M. C. *et al.* Nomenclature for Macrolide and Macrolide-Lincosamide-Streptogramin B Resistance Determinants. *Antimicrob Agents Chemother* **43**, 2823–2830 (1999).
23. Daly, M. M., Doktor, S., Flamm, R. & Shortridge, D. Characterization and Prevalence of MefA, MefE, and the Associated msr(D) Gene in Streptococcus pneumoniae Clinical Isolates. *J Clin Microbiol* **42**, 3570–3574 (2004).
24. Nunez-Samudio, V. & Chesneau, O. Functional interplay between the ATP binding cassette Msr(D) protein and the membrane facilitator superfamily Mef(E) transporter for macrolide resistance in Escherichia coli. *Research in Microbiology* **164**, 226–235 (2013).
25. Tatsuno, I. *et al.* Functional Predominance of msr(D), Which Is More Effective as mef(A)-Associated Than mef(E)-Associated, Over mef(A)/mef(E) in Macrolide Resistance in Streptococcus pyogenes. *Microbial Drug Resistance* **24**, 1089–1097 (2018).
26. Zhang, Y. *et al.* Predominant role of msr(D) over mef(A) in macrolide resistance in Streptococcus pyogenes. *Microbiology (Reading)* **162**, 46–52 (2016).
27. Del Grosso, M., Camilli, R., Iannelli, F., Pozzi, G. & Pantosti, A. The mef(E)-Carrying Genetic Element (mega) of Streptococcus pneumoniae: Insertion Sites and Association with Other Genetic Elements. *Antimicrob Agents Chemother* **50**, 3361–3366 (2006).
28. Del Grosso, M., Scotto d'Abusco, A., Iannelli, F., Pozzi, G. & Pantosti, A. Tn2009, a Tn916-Like Element Containing mef(E) in Streptococcus pneumoniae. *Antimicrob Agents Chemother* **48**, 2037–2042 (2004).
29. Chancey, S. T. *et al.* Composite mobile genetic elements disseminating macrolide resistance in Streptococcus pneumoniae. *Front. Microbiol.* **6**, (2015).
30. Iannelli, F. *et al.* Nucleotide sequence of conjugative prophage Φ1207.3 (formerly Tn1207.3) carrying the mef(A)/msr(D) genes for efflux resistance to macrolides in Streptococcus pyogenes. *Front Microbiol* **5**, (2014).
31. González-Zorn, B. *et al.* Genetic basis for dissemination of armA. *Journal of Antimicrobial Chemotherapy* **56**, 583–585 (2005).
32. Ambrose, K. D., Nisbet, R. & Stephens, D. S. Macrolide Efflux in Streptococcus pneumoniae Is Mediated by a Dual Efflux Pump (mel and mef) and Is Erythromycin Inducible. *Antimicrob Agents Chemother* **49**, 4203–4209 (2005).
33. Chancey, S. T. *et al.* Transcriptional Attenuation Controls Macrolide Inducible Efflux and Resistance in Streptococcus pneumoniae and in Other Gram-Positive Bacteria Containing mef/mel(msr(D)) Elements. *PLOS ONE* **10**, e0116254 (2015).
34. Ramu, H., Mankin, A. & Vazquez-Laslop, N. Programmed drug-dependent ribosome stalling. *Mol Microbiol* **71**, 811–824 (2009).
35. Sothiselvam, S. *et al.* Macrolide antibiotics allosterically predispose the ribosome for translation arrest. *Proc Natl Acad Sci U S A* **111**, 9804–9809 (2014).
36. de Block, T. *et al.* WGS of Commensal Neisseria Reveals Acquisition of a New Ribosomal Protection Protein (MsrD) as a Possible Explanation for High Level Azithromycin Resistance in Belgium. *Pathogens* **10**, 384 (2021).
37. Lu, C. *et al.* Phenotypic and Genetic Characteristics of Macrolide and Lincosamide Resistant Ureaplasma urealyticum Isolated in Guangzhou, China. *Curr Microbiol* **61**, 44–49 (2010).

38. Sharma, P. *et al.* Comparison of Antimicrobial Resistance and Pan-Genome of Clinical and Non-Clinical Enterococcus cecorum from Poultry Using Whole-Genome Sequencing. *Foods* **9**, 686 (2020).
39. Nikaido, H. Multidrug Resistance in Bacteria. *Annual Review of Biochemistry* **78**, 119–146 (2009).
40. Nikaido, H. & Pagès, J.-M. Broad-specificity efflux pumps and their role in multidrug resistance of Gram-negative bacteria. *FEMS Microbiol Rev* **36**, 340–363 (2012).
41. Datta, N., Hedges, R. W., Becker, D. & Davies, J. Plasmid-determined Fusidic Acid Resistance in the Enterobacteriaceae. *Microbiology,* **83**, 191–196 (1974).
42. Kannan, K. *et al.* The general mode of translation inhibition by macrolide antibiotics. *Proc Natl Acad Sci U S A* **111**, 15958–15963 (2014).
43. Vázquez-Laslop, N. & Mankin, A. S. How macrolide antibiotics work. *Trends Biochem Sci* **43**, 668–684 (2018).
44. Murina, V. *et al.* ABCF ATPases Involved in Protein Synthesis, Ribosome Assembly and Antibiotic Resistance: Structural and Functional Diversification across the Tree of Life. *Journal of Molecular Biology* **431**, 3568–3590 (2019).
45. Fürste, J. P. *et al.* Molecular cloning of the plasmid RP4 primase region in a multi-host-range tacP expression vector. *Gene* **48**, 119–131 (1986).
46. Lutz, R. & Bujard, H. Independent and Tight Regulation of Transcriptional Units in Escherichia Coli Via the LacR/O, the TetR/O and AraC/I1-I2 Regulatory Elements. *Nucleic Acids Res* **25**, 1203–1210 (1997).
47. Dubnau, D. Induction of ermC requires translation of the leader peptide. *EMBO J* **4**, 533–537 (1985).
48. Dersch, P., Khan, M. A., Mühlen, S. & Görke, B. Roles of Regulatory RNAs for Antibiotic Resistance in Bacteria and Their Potential Value as Novel Drug Targets. *Front. Microbiol.* **8**, (2017).
49. Banerjee, S., Chalissery, J., Bandey, I. & Sen, R. Rho-dependent Transcription Termination: More Questions than Answers. *J Microbiol* **44**, 11–22 (2006).
50. Ray-Soni, A., Bellecourt, M. J. & Landick, R. Mechanisms of Bacterial Transcription Termination: All Good Things Must End. *Annual Review of Biochemistry* **85**, 319–347 (2016).
51. Naville, M., Ghuillot-Gaudeffroy, A., Marchais, A. & Gautheret, D. ARNold: A web tool for the prediction of Rho-independent transcription terminators. *RNA Biology* **8**, 11–13 (2011).
52. Takada, H. *et al.* Expression of Bacillus subtilis ABCF antibiotic resistance factor VmlR is regulated by RNA polymerase pausing, transcription attenuation, translation attenuation and (p)ppGpp. *Nucleic Acids Res* gkac497 (2022) doi:10.1093/nar/gkac497.
53. Yakhnin, A. V. *et al.* NusG controls transcription pausing and RNA polymerase translocation throughout the Bacillus subtilis genome. *Proc Natl Acad Sci U S A* **117**, 21628–21636 (2020).
54. Shimizu, Y. *et al.* Cell-free translation reconstituted with purified components. *Nat Biotechnol* **19**, 751–755 (2001).
55. Hartz, D., McPheeters, D. S., Traut, R. & Gold, L. Extension inhibition analysis of translation initiation complexes. in *Methods in Enzymology* vol. 164 419–425 (Academic Press, 1988).
56. Meydan, S. *et al.* Retapamulin-Assisted Ribosome Profiling Reveals the Alternative Bacterial Proteome. *Molecular Cell* **74**, 481-493.e6 (2019).

57. Muto, H., Nakatogawa, H. & Ito, K. Genetically Encoded but Nonpolypeptide Prolyl-tRNA Functions in the A Site for SecM-Mediated Ribosomal Stall. *Molecular Cell* **22**, 545–552 (2006).
58. Seip, B. & Innis, C. A. How Widespread is Metabolite Sensing by Ribosome-Arresting Nascent Peptides? *Journal of Molecular Biology* **428**, 2217–2227 (2016).
59. Vázquez-Laslop, N. *et al.* Role of antibiotic ligand in nascent peptide-dependent ribosome stalling. *Proc. Natl. Acad. Sci. U.S.A.* **108**, 10496–10501 (2011).
60. Hansen, J. L. *et al.* The Structures of Four Macrolide Antibiotics Bound to the Large Ribosomal Subunit. *Molecular Cell* **10**, 117–128 (2002).
61. Mao, J. C. & Robishaw, E. E. Effects of macrolides on peptide-bond formation and translocation. *Biochemistry* **10**, 2054–2061 (1971).
62. Poulsen, S. M., Kofoed, C. & Vester, B. Inhibition of the ribosomal peptidyl transferase reaction by the mycarose moiety of the antibiotics carbomycin, spiramycin and tylosin1 1Edited by D. E. Draper. *Journal of Molecular Biology* **304**, 471–481 (2000).
63. Emmanuel, J. S., Sengupta, A., Gordon, E. R., Noble, J. T. & Cruz-Vera, L. R. The regulatory TnaC nascent peptide preferentially inhibits release factor 2-mediated hydrolysis of peptidyl-tRNA. *J Biol Chem* **294**, 19224–19235 (2019).
64. Ohashi, Z. *et al.* Characterization of C+ located in the first position of the anticodon of Escherichia coli tRNAMet as N4-acetylcytidine. *Biochimica et Biophysica Acta (BBA) - Nucleic Acids and Protein Synthesis* **262**, 209–213 (1972).
65. Varshney, U., Lee, C. P. & RajBhandary, U. L. From elongator tRNA to initiator tRNA. *PNAS* **90**, 2305–2309 (1993).
66. Pierson, W. E. *et al.* Uniformity of Peptide Release Is Maintained by Methylation of Release Factors. *Cell Reports* **17**, 11–18 (2016).
67. Schmeing, T. M., Huang, K. S., Strobel, S. A. & Steitz, T. A. An induced-fit mechanism to promote peptide bond formation and exclude hydrolysis of peptidyl-tRNA. *Nature* **438**, 520–524 (2005).
68. Arenz, S. *et al.* Molecular basis for erythromycin-dependent ribosome stalling during translation of the ErmBL leader peptide. *Nature Communications* **5**, 3501 (2014).
69. Lovmar, M. *et al.* The Molecular Mechanism of Peptide-mediated Erythromycin Resistance *. *Journal of Biological Chemistry* **281**, 6742–6750 (2006).
70. Tenson, T., Xiong, L., Kloss, P. & Mankin, A. S. Erythromycin Resistance Peptides Selected from Random Peptide Libraries*. *Journal of Biological Chemistry* **272**, 17425–17430 (1997).
71. Koch, M., Willi, J., Pradère, U., Hall, J. & Polacek, N. Critical 23S rRNA interactions for macrolide-dependent ribosome stalling on the ErmCL nascent peptide chain. *Nucleic Acids Res* **45**, 6717–6728 (2017).
72. Vázquez-Laslop, N., Ramu, H., Klepacki, D., Kannan, K. & Mankin, A. S. The key function of a conserved and modified rRNA residue in the ribosomal response to the nascent peptide. *EMBO J* **29**, 3108–3117 (2010).
73. Vimberg, V. *et al.* Ribosome-Mediated Attenuation of vga(A) Expression Is Shaped by the Antibiotic Resistance Specificity of Vga(A) Protein Variants. *Antimicrobial Agents and Chemotherapy* **64**, (2020).
74. Jacquet, E. *et al.* ATP Hydrolysis and Pristinamycin IIA Inhibition of the Staphylococcus aureus Vga(A), a Dual ABC Protein Involved in Streptogramin A Resistance *. *Journal of Biological Chemistry* **283**, 25332–25339 (2008).
75. Mayford, M. & Weisblum, B. Conformational alterations in the ermC transcript in vivo during induction. *EMBO J* **8**, 4307–4314 (1989).

1117 76. Dar, D. *et al.* Term-seq reveals abundant ribo-regulation of antibiotics resistance in
1118 bacteria. *Science* **352**, aad9822 (2016).
1119 77. Koberska, M. *et al.* Beyond Self-Resistance: ABCF ATPase LmrC Is a Signal-
1120 Transducing Component of an Antibiotic-Driven Signaling Cascade Accelerating
1121 the Onset of Lincomycin Biosynthesis. *mBio* **12**, e0173121 (2021).
1122 78. Ohki, R., Tateno, K., Takizawa, T., Aiso, T. & Murata, M. Transcriptional
1123 Termination Control of a Novel ABC Transporter Gene Involved in Antibiotic
1124 Resistance in Bacillus subtilis. *J Bacteriol* **187**, 5946–5954 (2005).
1125 79. Dunkle, J. A., Xiong, L., Mankin, A. S. & Cate, J. H. D. Structures of the Escherichia
1126 coli ribosome with antibiotics bound near the peptidyl transferase center explain
1127 spectra of drug action. *Proc Natl Acad Sci U S A* **107**, 17152–17157 (2010).
1128 80. Desai, N. *et al.* Elongational stalling activates mitoribosome-associated quality
1129 control. *Science* **370**, 1105–1110 (2020).
1130 81. Golubev, A. *et al.* Cryo-EM structure of the ribosome functional complex of the
1131 human pathogen Staphylococcus aureus at 3.2 Å resolution. *FEBS Letters* **594**,
1132 3551–3567 (2020).
1133 82. Li, W. *et al.* Structural basis for selective stalling of human ribosome nascent chain
1134 complexes by a drug-like molecule. *Nat Struct Mol Biol* **26**, 501–509 (2019).
1135 83. Croucher, N. J. *et al.* Rapid pneumococcal evolution in response to clinical
1136 interventions. *Science* **331**, 430–434 (2011).
1137 84. Miller, J. R. *GraphPad Prism Version 4.0 Step-by-Step Examples*. vol. GraphPad
1138 Software Inc., San Diego (GraphPad Software Inc., San Diego, 2003).
1139 85. Stead, M. B. *et al.* RNAsnap^{TM}: a rapid, quantitative and inexpensive, method for
1140 isolating total RNA from bacteria. *Nucleic Acids Res* **40**, e156 (2012).
1141 86. Seefeldt, A. C. *et al.* The proline-rich antimicrobial peptide Onc112 inhibits
1142 translation by blocking and destabilizing the initiation complex. *Nature Structural &*
1143 *Molecular Biology* **22**, 470–475 (2015).
1144 87. Zheng, S. Q. *et al.* MotionCor2 - anisotropic correction of beam-induced motion for
1145 improved cryo-electron microscopy. *Nat Methods* **14**, 331–332 (2017).
1146 88. Zhang, K. Gctf: Real-time CTF determination and correction. *J Struct Biol* **193**, 1–
1147 12 (2016).
1148 89. Zivanov, J. *et al.* New tools for automated high-resolution cryo-EM structure
1149 determination in RELION-3. *eLife* **7**, e42166 (2018).
1150 90. Kucukelbir, A., Sigworth, F. J. & Tagare, H. D. The Local Resolution of Cryo-EM
1151 Density Maps. *Nat Methods* **11**, 63–65 (2014).
1152 91. Emsley, P. & Cowtan, K. Coot: model-building tools for molecular graphics. *Acta*
1153 *Cryst D* **60**, 2126–2132 (2004).
1154 92. Liebschner, D. *et al.* Macromolecular structure determination using X-rays,
1155 neutrons and electrons: recent developments in Phenix. *Acta Cryst D* **75**, 861–877
1156 (2019).
1157 93. Boccaletto, P. *et al.* MODOMICS: a database of RNA modification pathways. 2017
1158 update. *Nucleic Acids Res* **46**, D303–D307 (2018).
1159 94. Bourgeois, G. *et al.* Structural basis of the interaction between cyclodipeptide
1160 synthases and aminoacylated tRNA substrates. *RNA* **26**, 1589–1602 (2020).
1161 95. Waterhouse, A. M., Procter, J. B., Martin, D. M. A., Clamp, M. & Barton, G. J.
1162 Jalview Version 2—a multiple sequence alignment editor and analysis workbench.
1163 *Bioinformatics* **25**, 1189–1191 (2009).
1164 96. Schindelin, J. *et al.* Fiji: an open-source platform for biological-image analysis.
1165 *Nature Methods* **9**, 676–682 (2012).

97. Goddard, T. D. *et al.* UCSF ChimeraX: Meeting modern challenges in visualization and analysis. *Protein Sci* **27**, 14–25 (2018).
98. Pettersen, E. F. *et al.* UCSF Chimera—A visualization system for exploratory research and analysis. *Journal of Computational Chemistry* **25**, 1605–1612 (2004).

1171

FIGURE 1

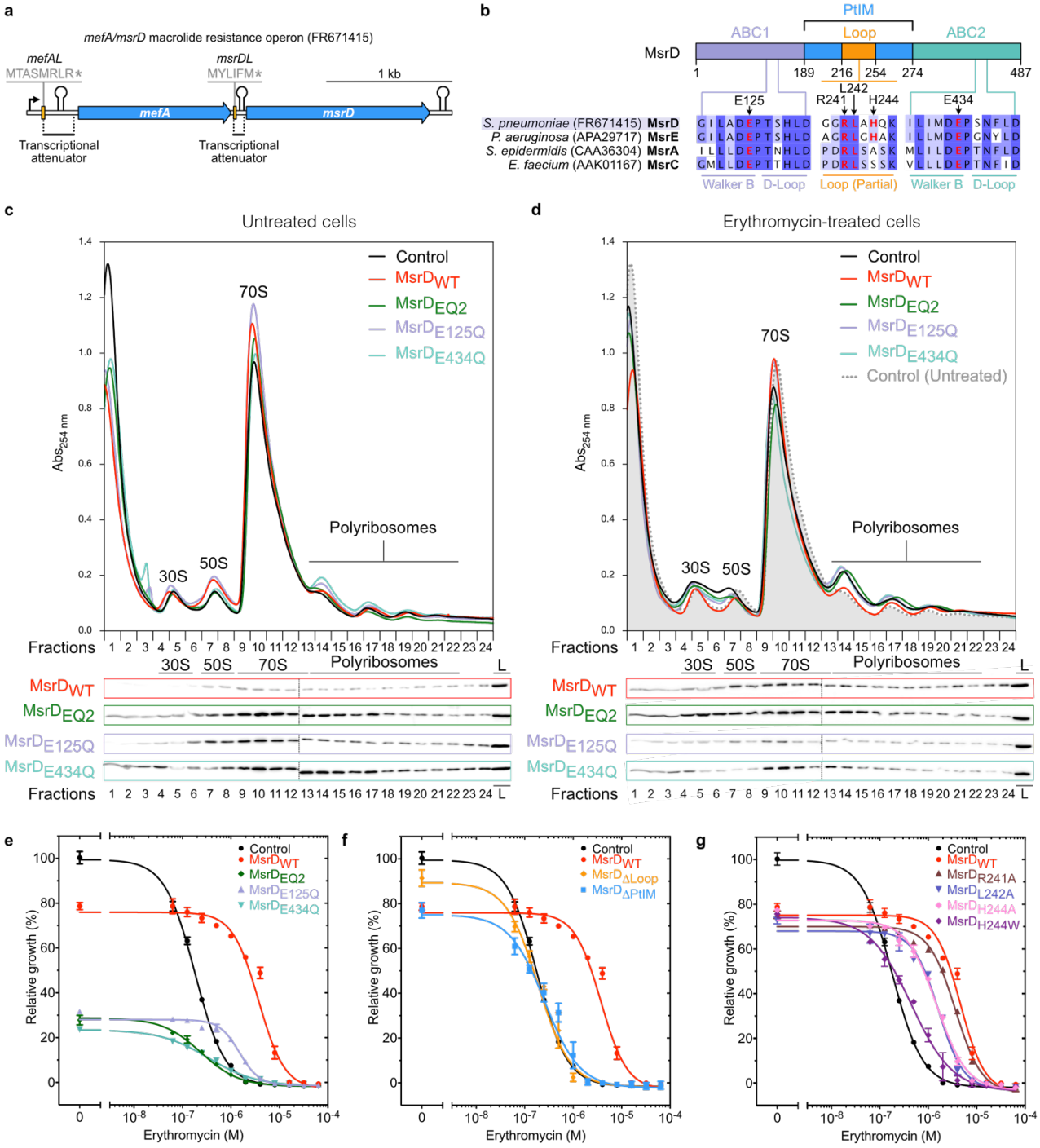

1172

FIGURE 2

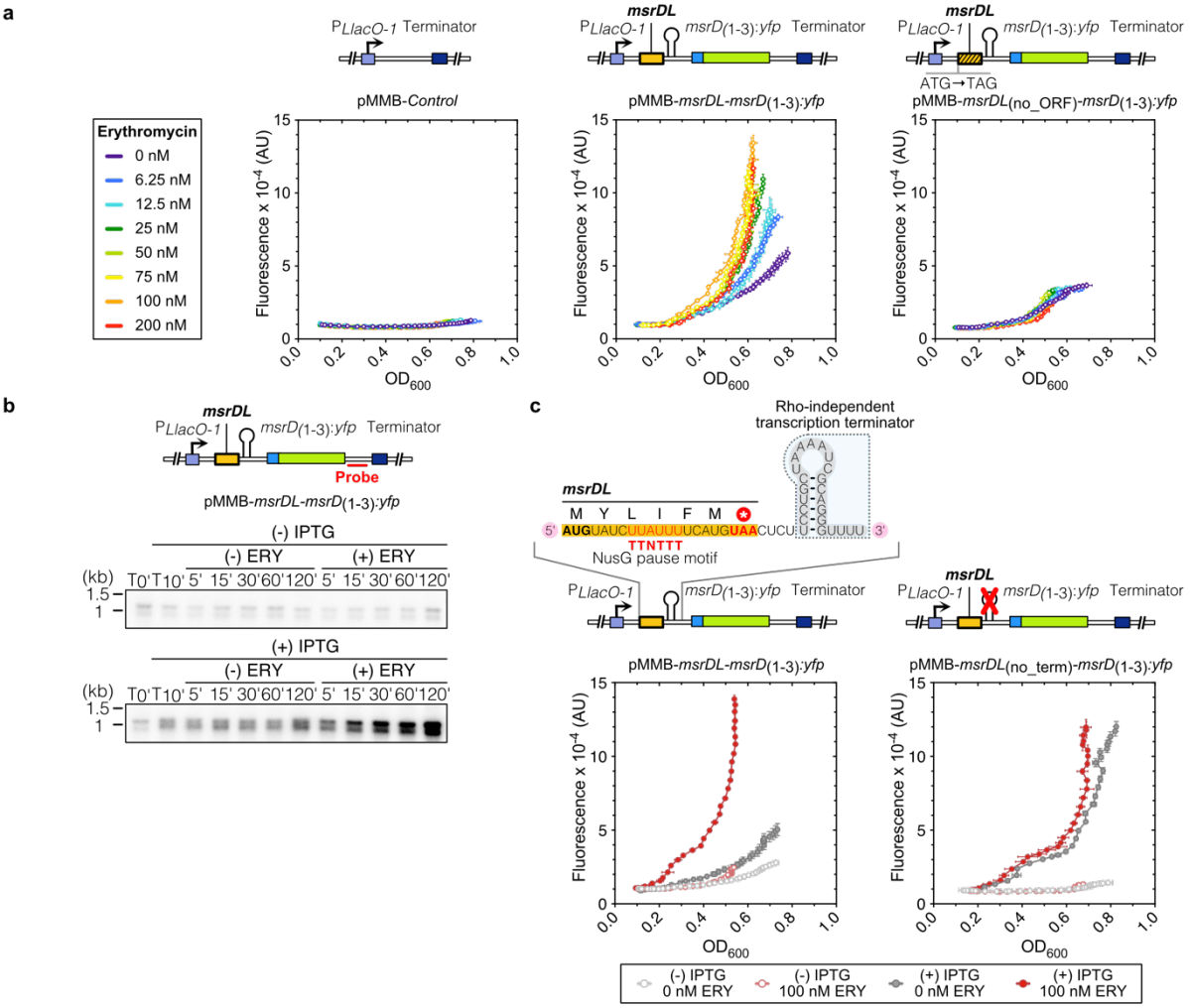

1173

FIGURE 3

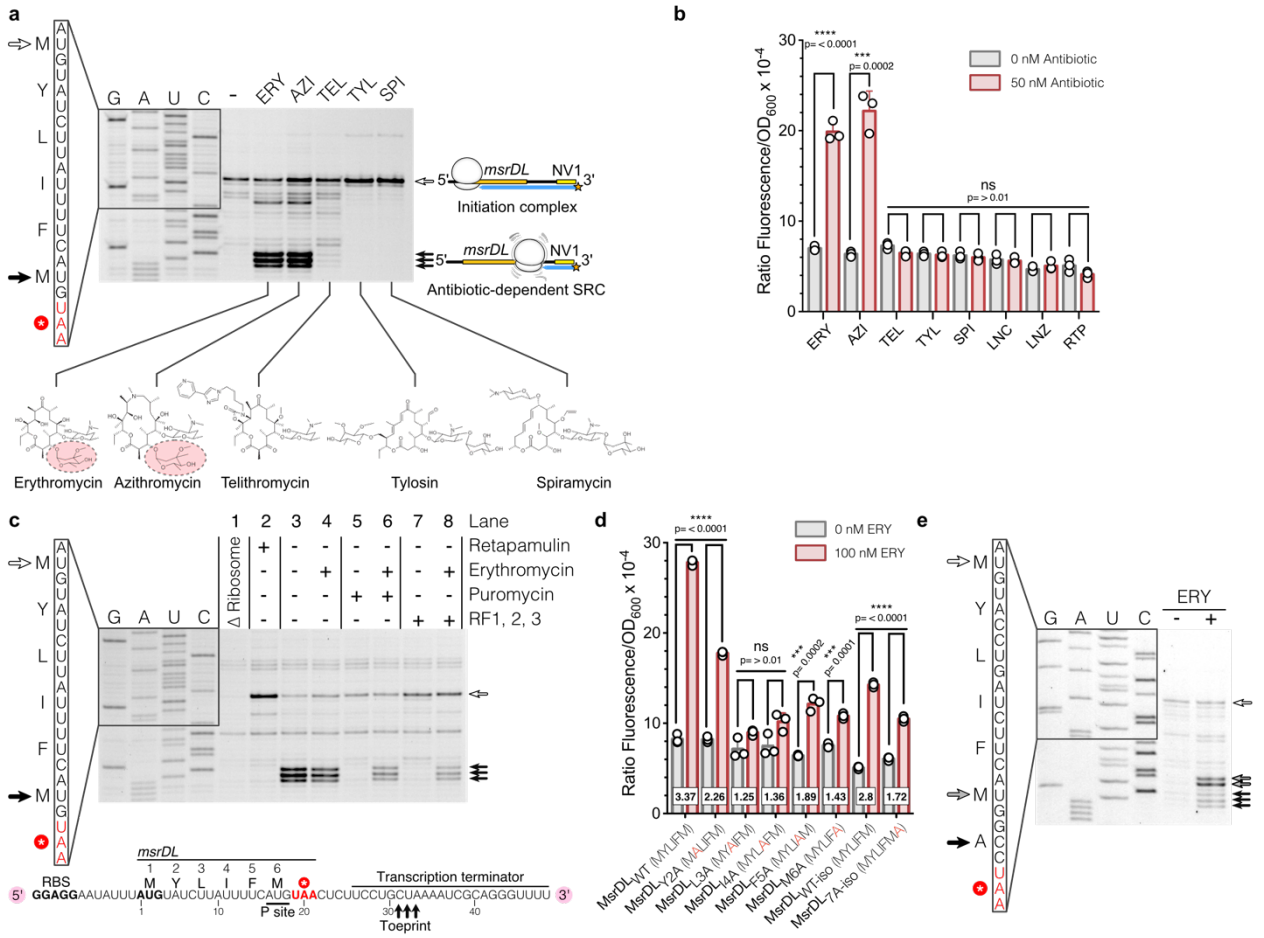

1174

FIGURE 4

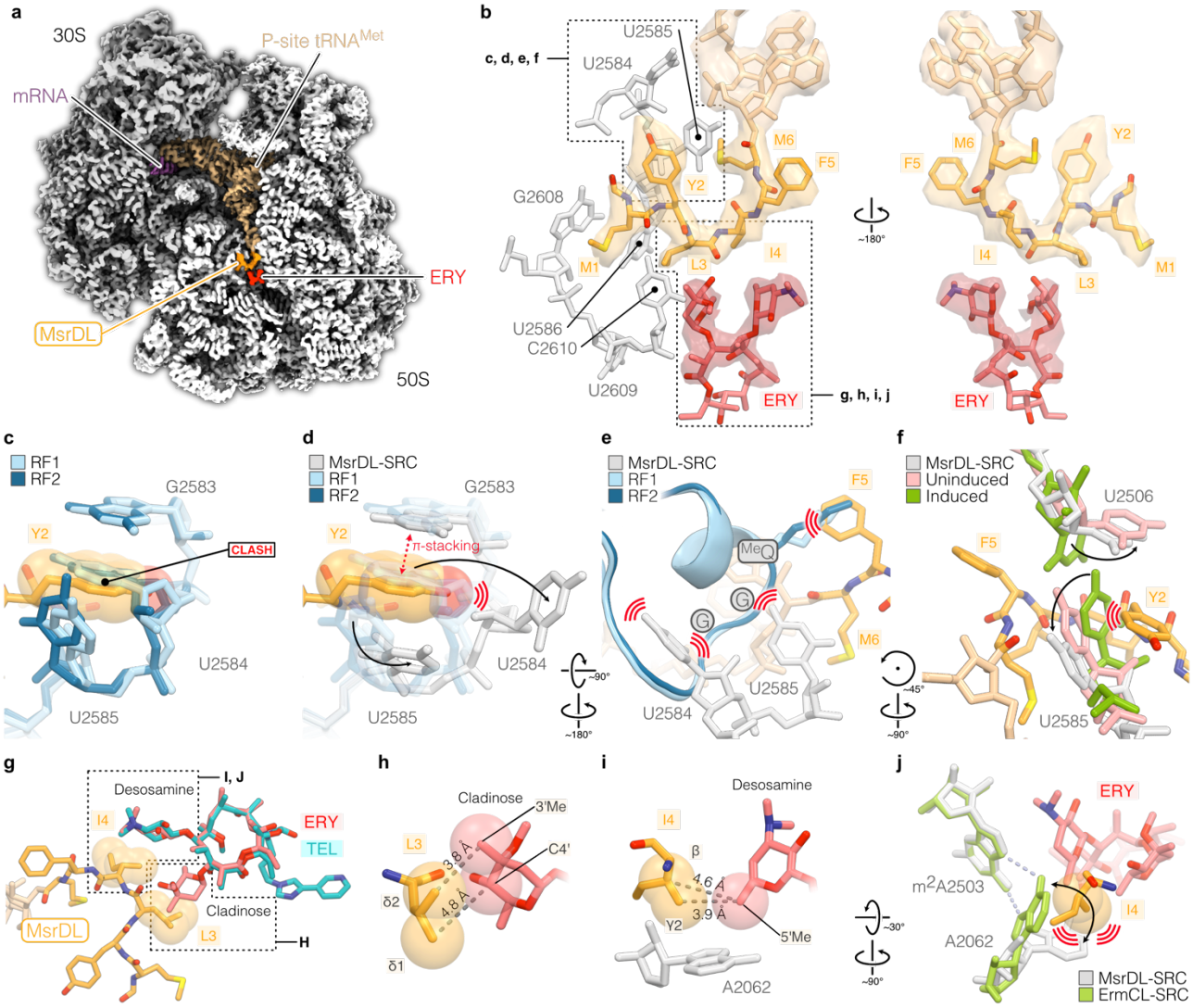

1175

FIGURE 5

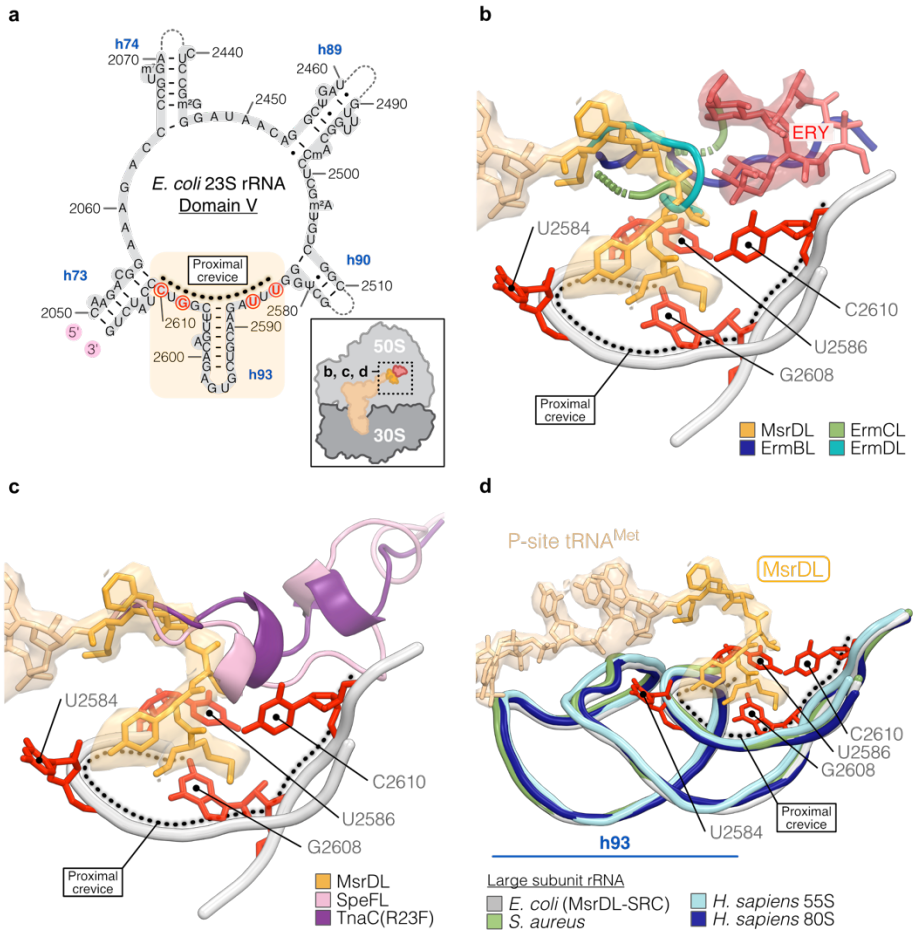

1176
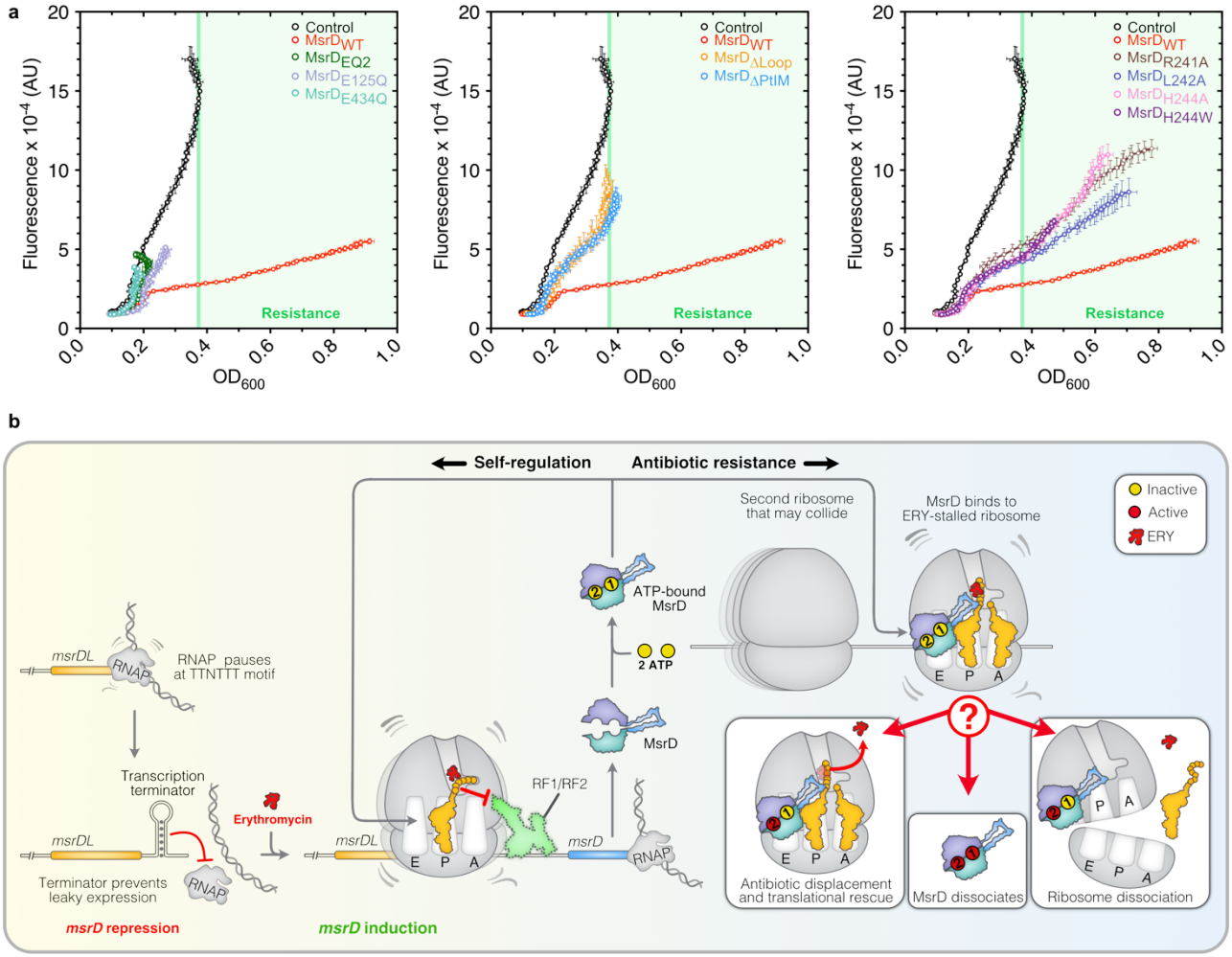
FIGURE 6